METAMORPHISM

IN THE

PRINCE ALBERT GROUP

CHURCHILL PROVINCE, DISTRICT OF KEEWATIN, N.W.T.

METAMORPHISM

IN THE

PRINCE ALBERT GROUP

CHURCHILL PROVINCE, DISTRICT OF KEEWATIN, N.W.T.

By

JOHN MARVIN WOLFF

Submitted to the Department of Geology

in Partial Fulfilment of the Requirements

for the Degree

Honours Bachelor of Science

McMaster University

April, 1974

HONOURS BACHELOR OF SCIENCE (1974)
(Geology)

McMASTER UNIVERSITY
Hamilton, Ontario.

TITLE: Metamorphism in the Prince Albert Group, Churchill Province, District of Keewatin, N.W.T.

AUTHOR: John Marvin Wolff

SUPERVISORS: Professors R. H. McNutt and H. D. Grundy

NUMBER OF PAGES: xii, 118.

SCOPE AND CONTENTS:

A sequence of metasedimentary rocks comprising the Prince Albert Group, within and to the southwest of the Ellice Hills, District of Keewatin, N.W.T., was studied. Petrographic examination of the four major facies present -- quartzites, greywacke-paragneisses, meta-ultrabasics and iron formation was carried out and geochemical whole rock data was obtained using X.R.F. methods.

Metamorphism occurred during the Hudsonian orogeny and came in three distinct pulses. These pulses are evident in thin section. The first pulse is characterized by the formation of garnet poikiloblasts and a biotite foliation; the second by a stronger biotite and hornblende

foliation accompanied by quartz and muscovite porphyroblasts, and the third pulse is characterized by the growth of fibrolite needles. The last pulse of metamorphism shows that fibrolite and orthoclase formed from the dehydration of muscovite in the presence of quartz. Thus, a pressure and temperature regime for this event can be inferred from published experimental studies. These indicate that P_{H_2O} ranged from 2.0 to 3.5 Kbars and that temperature ranged from 640° ± 10°C to 670° ± 10°C. Previous pulses may have had higher pressure ranges but certainly lower temperature ranges prevailed. The present metamorphic grade of the Prince Albert Group displays mineral assemblages indicative of the Sillimanite-orthoclase-almandine Subfacies of the Almandine-amphibolite Facies as defined by Winkler (1967).

Structural deformation is closely associated with metamorphism. At least three periods of deformation have occurred. The first is evident in thin section by the S_1 foliation and parallel trains of sialic material in garnet poikiloblasts. The second period of deformation caused the rotation of the above garnets, plus formation of the F_2 isoclinal folds, S_2 biotite foliation, crenulation of the S_1 foliation and the formation of muscovite-quartz porphyroblasts. The third period of deformation is responsible for the F_3 folding, warping of the F_2 axial trace and the anisotropic growth of fibrolite.

Figure 1. Land of the Midnight Sun. Photograph taken at 2400 hrs., June 27th, 1973, Latitude 67°10'N.

Figure 2. A young caribou buck streaking across tundra in the Prince Albert Group.

Geochemical whole rock analysis shows that these rocks had protoliths of several types, including miogeosynclinal sandstones and clays, and eugeosynclinal greywackes and iron formations. Basaltic material also entered the stratigraphic column.

ACKNOWLEDGEMENTS

First, and foremost, the writer would like to express his gratitude to Dr. F.H.A. Campbell of the Geological Survey of Canada for allowing collection of the field data and samples during the 1973 field season.

The guidance and constructive advice provided by the author's supervisors, Drs. R.H. McNutt and H.D. Grundy is also appreciated.

Thanks goes to Mr. J. Whorwood for assistance in preparation of the photographs, and to Mr. D. Falkiner for preparation of the thin sections. Also, Mr. M. Marchand and Mr. H. Baitis are to be thanked for their assistance in the whole rock analysis. A word of thanks goes to J. Kamenof for critical editing of the manuscript and to Mrs. A. Antanavicius who kindly undertook typing of the manuscript.

The meticulous inking of the petrographic sketches was carried out by Mr. and Mrs. W.P. Binney. The author is extremely grateful for their assistance.

Last, but by no means least, the author is indebted to the Bickell Foundation which provided funds to cover part of the cost of typing, copying and binding of the thesis.

TABLE OF CONTENTS

		PAGE
CHAPTER I	INTRODUCTION	
	i) Location and Accessibility	1
	ii) Previous Work	3
	iii) Statement of Problem	3
	iv) Method of Sampling	4
CHAPTER II	GENERAL GEOLOGY	
	i) Regional Setting	6
	a) Orthogneisses	6
	b) Granites	6
	c) Prince Albert Group Metasedimentary Rocks	8
	c-i) Quartzite Sequence	8
	c-ii) Greywacke-Paragneiss Sequence	10
	d) Meta-Ultrabasic Rocks	12
	ii) Stratigraphy	13
	iii) Structure	14
	a) Regional Setting	14
	b) Details of Structural Deformation	15
	c) Faults, Dykes and Sills	17

		PAGE
CHAPTER III	TEXTURES AND MINERALOGY	
	i) Quartzite Sequence	18
	ii) Greywacke-Paragneiss Sequence	24
	a) Muscovite-bearing Paragneisses	24
	b) Almandine Garnet-bearing Paragneisses	27
	c) Hornblende-bearing Paragneisses	28
	d) Iron Formation	31
	iii) Meta-Ultrabasic Rocks	31
CHAPTER IV	PETROCHEMISTRY	
	i) Analytical and Data Reduction Methods	33
	ii) Chemographic Plots	37
	a) Al_2O_3-Na_2O-K_2O Plot	37
	b) AFM Plot	37
	c) ACF Plot	40
	iii) Chemical Evidence of Prince Albert Group Protoliths	42
CHAPTER V	METAMORPHISM	
	i) Regional Grade of Metamorphism of the Prince Albert Group	45
	ii) Metamorphism of the Prince Albert Group-Ellice Hills Sheet	45

		PAGE
	a) Mineral Assemblages Present	46
	b) Metamorphic Mineral Reactions Present	47
iii)	Pressure and Temperature of Metamorphism	50
iv)	Chemical Considerations With Respect to Metamorphism	53
v)	Structural Considerations With Respect to Metamorphism	54
vi)	Tectono-Thermo-Time Relations	55
vii)	Contribution Towards an Orogenic Model	58

REFERENCES 60

APPENDICES 64

LIST OF TABLES

TABLE		PAGE
I	Mineral Tally	19
II	Whole Rock Analysis in Weight % Oxides (Normalized)	35

LIST OF FIGURES

FIGURE		PAGE
1.	Land of the Midnight Sun	v
2.	Caribou in the PAG	v
3.	Location Map	3
4.	General Geology of the PAG, Ellice Hills Sheet	5
5.	Quartzite and Greywacke-Paragneiss Sequences, at J73-040	7
6.	Quartzite and Greywacke-Paragneiss Sequences, at T-bar Lake	7
7.	Sillimanite-Quartz-Pebble Conglomerate in the Quartzite Sequence	9
8.	Banded Quartz-Magnetite Iron Formation	11
9.	Greywacke-Paragneiss Sequence	11
10.	Paragneiss Deformation	16
11.	Sillimanite Porphyroblast from J73-061, X-nicols	21
12.	Sillimanite Porphyroblast from J73-061, Plane Polarized Light	21
13.	Dehydration Reaction of Muscovite, J73-032	23
14.	Fibrolite at 400X Magnification	23
15.	Isoclinal Folding in J73-048	26
16.	Garnet Poikiloblast in J73-050-2, X-nicols	29
17.	Garnet Poikiloblast in J73-050-2, Plane Polarized Light	29
18.	Al_2O_3-K_2O-Na_2O Plot	38

FIGURE		PAGE
19.	AFM Plot	39
20.	ACF Plot	41
21.	MgO-CaO Plot	43
22.	Al_2SiO_5 Stability Field	52
23.	Tectono-Thermo-Time Plot	57

CHAPTER I

INTRODUCTION

i) Location and Accessibility:

The Prince Albert Group, (PAG), of metasedimentary rocks is located in the northeast portion of the Churchill Province of the Canadian Shield. These Pre-Cambrain rocks cut across Melville Peninsula, District of Franklin, (Frisch, 1974; Heywood, 1974), and crop out on the western shore of Committee Bay, south of Cape Weynton, to a point northwest of Baker Lake, District of Keewatin. The specific section of the group examined for this study is bounded by the Ellice Hills map sheet 56P, 1:250,000. The actual meridians and parallels of boundary are Latitude 67°10'N, Longitude 90°00'W, and Latitude 67°35'N, Longitude 88°00'W. The general trend of the rocks of the PAG is southwest to northeast. The western limit is very dubious as the rocks grade into similar, but not necessarily PAG rocks, in this area, see Fig. 3.

Access to the study area is possible by two settlements, Repulse Bay, District of Franklin, approximately one-hundred miles to the southeast, and Baker Lake, District of Keewatin, approximately three hundred miles to the southwest. The area studied is well within the Barren Grounds of the Northwest Territories and accessible only by STOL aircraft or helicopter.

LOCATION MAP

Scale

0 MILES 150 — 0 KM. 150

Study Area

Fig. 3.

ii) Previous Work:

The study area has been mapped on a reconnaissance scale, (8 miles to 1 inch), as part of a larger mapping project between Baker Lake and Melville Peninsula (Heywood, 1961, 1966; Wright, 1967). A later, more detailed mapping project, (1 mile to 1 inch), was started in 1972, (Campbell, 1973; Frisch, 1973; Schau, 1973), and included the area studied plus portions to the east and west. Results from the 1972 study indicated the PAG bears mineral assemblages indicative of the Amphibolite grade of metamorphism. The 1972 study also indicated that the rocks become more volcanic to the west of the present study area (Schau, 1973). The latest work in the area studied was a continuation of the mapping project started in 1972, carried out by F. H. A. Campbell in the field season of 1973. Preliminary results of this work have been published (Campbell, 1974).

iii) Statement of Problem:

The PAG of metasedimentary rocks is thought to be Aphebian in age with the latest metamorphic event being the Hudsonian orogeny (1800 ± 50 M.Y.). This however, should not discount the fact that possible metamorphic events occurring during the Kenoran orogeny, (2615 ± 75 M.Y.), may have effected these rocks,(radiometric dates from Stockwell, 1972). The metamorphic grade of these rocks is believed to be Almandine-amphibolite, but detailed work in this field has not been attempted to date.

The aim of the present study is to determine the metamorphic history of a part of the metasedimentary rocks of the PAG by examing a representative suite of the group, with special emphasis being placed on its petrography and petrochemistry. Representative chemographic diagrams will be presented.

iv) Method of Sampling:

To obtain a representative suite from the PAG, sampling was carried out at four different areas, each representing a section across strike. These sections are namely the Kellett River, the T-bar Lake, the Curtis River and the Committee Bay sections. The sample locations are shown on the accompanying map (see Fig. 4). UTM coordinates were taken from photomaps (scale 1:50,000), of the area. As can be seen, the first two sections represent the western and eastern parts of the western fault block, and the third and fourth the central and eastern fault blocks respectively. The geology on the accompanying map is taken from Heywood's reconnaissance geology of the area (1966). This map shows general trends and boundaries of the group. A more detailed map of the study area is presently being compiled by Campbell.

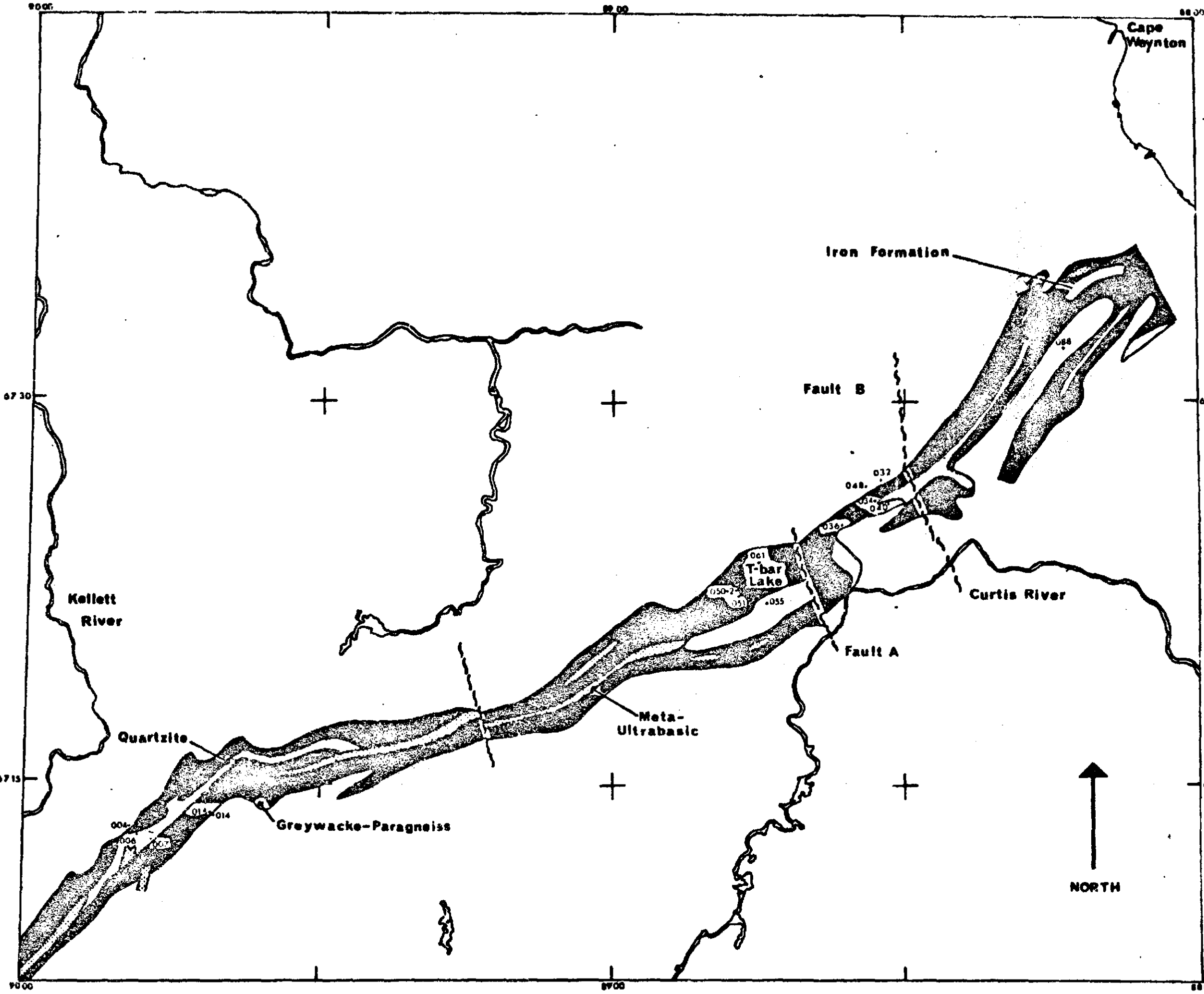

GENERAL GEOLOGY OF THE PRINCE ALBERT GROUP, (ELLICE HILLS SHEET)

miles 0 10
km. 0 10

after W.W. Heywood, 1966.

Fig. 4.

CHAPTER II

GENERAL GEOLOGY

i) Regional Setting:

The major rock types found in the area can be divided into four major categories, the orthogneisses, the granites, the PAG metasedimentary rocks, and the meta-ultrabasic rocks.

a) Orthogneisses:

The orthogneisses are of two main types, granodioritic and granitic gneiss. Of the two, the granodioritic type is the most common. It appears to be younger than the PAG as suggested by the metasedimentary (probably PAG) xenoliths found in the granodioritic gneisses, and by transition zones between the PAG paragneisses and the granodioritic gneisses. The granodioritic gneisses often invade and pinch the PAG, and to the east occur as prominent sills (Campbell, 1974). Foliation trends in the granodioritic gneiss are generally irregular. The granitic gneiss is minor and only mentioned in this report for completeness.

b) Granites:

The granites found in the area may be younger than the PAG. They are generally massive to weakly foliated and biotite is a common mafic mineral constituent. These granites are usually associated with the granodioritic gneiss but actual contacts between the two are often unclear and some may be gradational. In some localities the granite appears to be in contact with the PAG metasedimentary rocks.

Figure 5. Looking northeast from station J73-040. The large ridge to the left is the quartzite sequence while the hills to the right, the rock in the foreground, and the rock below the snow ridge on the left is the greywacke-paragneiss sequence. The lake is about 1/5 mile wide.

Figure 6. Looking north from the south shore of T-bar Lake. The ridge in the background with the snowbank touching the lake is the quartzite sequence. To the south of the lake is the greywacke-paragneiss sequence.

c) PAG Metasedimentary Rocks:

The northeast trending group of metasedimentary rocks can be divided into two major sequences, the quartzite sequence and the greywacke sequence (Campbell, 1974).

c-i) Quartzite Sequence:

The quartzite sequence is the most resistant rock type in the area forming the topographic ridge which is essentially continuous from Kellett River to fault B (see Figs. 5 and 6). The quartzite sequence can be divided into three subfacies quartzite, knotted quartzite and greywacke (after Campbell, 1974).

The quartzite of the belt is very white and contains quartz, a white mica (muscovite) and locally a brilliant green mica (fuchsite). Where the latter mineral is found ultrabasic rocks are in contact with the quartzite. A "conglomeratic" quartzite was also observed (see Fig. 7). This rock contains white quartz pebbles in a matrix of fine grained quartz and fibrolite. Some quartzites show iron staining. This staining is both red (hematitic) and rust-brown (pyritic).

The knotted quartzite shows prominent porphyroblasts of sillimanitic material in a matrix of fine grained quartz grains. Sillimanite knots were also observed in some greywackes of the quartzite sequence.

The greywackes of the quartzite sequence are minor and contain quartz, feldspar, muscovite and biotite and occasionally fibrolite. An example of such a rock is the greywacke form the quartzite sequence at T-bar Lake (J73-061). These minor greywacke units are laterally continuous

Figure 7. Quartz-pebble "conglomerate", taken at station J73-006. Adjacent to the hammer one can see quartz pebbles, and knots which are sillimanitic also exist. Fuchsite is the mica found here.

with the quartzites and probably represent a facies change.

East of fault B a notable amount of greywacke is found, but little quartzite. Perhaps this too is indicative of a lateral change in facies.

Structurally, the quartzite sequence possesses more shallow dips than the greywacke sequence and shows less deformation. However, the absence of a colour contrast within the quartzite sequence might mask any infolding present. Also, the quartzite sequence contains a much smaller proportion of mafic minerals than the greywacke sequence. These characteristics may suggest that the quartzite sequence is the youngest member of the PAG.

c-ii) Greywacke-Paragneiss Sequence:

The greywacke-paragneiss sequence represents the remainder of the metasedimentary rocks of the PAG. These include quartzo-feldspathic-biotite paragneissic greywackes plus iron formations.

The paragneisses are continuous over the length of the "belt" and possess mineral assemblages reminiscent of greywackes. Hand specimen investigation shows quartz, plagioclase, biotite, and occasionally almandine or sillimanite-fibrolite occur. Paragneisses possessing almandine are often situated in the vicinity of iron formations.

The iron formations appear to exist in two forms, one associated only with paragneisses and greywackes, and the other only with ultrabasic rocks (Campbell, 1974). Both iron formations are composed of interlayered quartz and magnetite (see Fig. 8). These prove to be useful marker horizons in the western part of the area studied. East of fault B, however,

Figure 8. An example of the banded quartz-magnetite (light and dark layers) iron formation. This particular one is associated with the greywacke-paragneiss sequence.

Figure 9. An example of the migmatitic veinlets in the greywacke-paragneiss sequence taken at station J73-004.

they cannot be utilized to the same advantage.

Small migmatitic veinlets and thin pegmatitic sills are found locally within paragneissic rocks. Occasionally these pegmatites show boudinage structure and strike parallel to the predominant foliation (see Fig. 9).

d) Meta-Ultrabasic Rocks:

The fourth major rock type is the meta-ultrabasic rocks or amphibolites. These are part of the PAG and are included as a subdivision of the greywacke sequence by Campbell (1974). These amphibolites are most commonly associated with the iron formation and locally with the quartzite sequence, mentioned above. When found with the iron formation, the amphibolite may contain xenoliths of the iron formation and is locally infolded with the iron formation. Periodically the amphibolite is interlayered with and transposed along the foliation plane into garnetiferous greywacke. Some of the amphibolites are known to display relict pillow structures with possible chill margins, while others are massive. Locally the massive amphibolites are interlayered with chloritic schists. This would seem to suggest that the amphibolites originated from volcanic flows and the chloritic schists possibly ash falls. The ultrabasic rocks described above are most prominent west of fault A (see Fig. 4). East of fault A an amphibolite is found but it is to the north of the "belt", well outside the main portion of the PAG (Campbell, 1974). It is possible that this more northerly ultrabasic volcanic of the central and eastern block is not the same age as that of the western block.

ii) Stratigraphy:

The age of the PAG is believed to be Aphebian based on the following criteria. First, the area contains a quartzite sequence which is not known to occur in any other Archean greenstone sequence (Davidson, 1972). Secondly, the area contains northwest trending diabase dykes but no northeast trending diabase dykes. Diabase dykes of both orientations have been found in the Kaminak Subprovince which is adjacent to and south of the area where the PAG occurs. These diabase dykes have been dated at 2330 ± 200 M.Y. and 1690 ± 55 M.Y. for the northeast and northwest types respectively (Davidson, 1970). The northwest trending dykes of the area studied are thought to be of the same age as those of the Kaminak Subprovince as they continue into the orthogneisses between the two, hence appearing to be a part of a larger swarm of northwest trending diabase dykes. Thus, it is reasonable to deduce that the age of the PAG is post-Kenoran (i.e. northeast trending dykes of the Kaminak Subprovince), and pre-northwest trending dykes of both subprovinces.

The true stratigraphic correlation of the area studied is unknown as insufficient stratigraphic evidence exists. However, time relations based on structural evidence are possible and provide the following paragenetic sequence: older basement orthogneisses (possibly remobilized and now appear as foliated orthogneisses), greywacke-paragneiss sequence of the PAG, quartzite sequence of the PAG, meta-ultrabasic rocks of the

PAG, orthogneisses, weakly foliated to massive granites (possibly associated with the pegmatite dykes and sills), and northwest trending diabase dykes. Pleistocene marine clays are known to lay unconformably over the PAG in the eastern block. Throughout the area it is common to find glacial till, boulder fields and eskers unconformably resting on the Pre-Cambrian rocks.

iii) Structure:

a) Regional Setting:

The gross structural trends of the Churchill Province are southwest-northeast with two main dyke sets, one trending northwest and the other northeast. The PAG fits into the general trend of the Churchill Province. The long axis of the group trends northeasterly and is cut locally by northwest trending diabase dykes. The structure of the PAG is basically that of a synform which has been pinched by younger orthogneisses and granites. Evidence of the synform structure is given by the change in sense of the drag folds from asymmetrical "Z" to "S" without change in plunge as one moves across strike. Deformation within the area studied is most prominent in the paragneisses and iron formations of the PAG. Such strain features as isoclinal chevron "kink" folds, two sets of isoclinal folds, asymmetrical "Z" and "S" drag folds, crenulated foliation and warped axial planes are exhibited in these rocks.

b) Details of Structural Deformation:

Deformation in the study area has occurred in at least three distinct periods (Campbell, 1974). The first, D_1, is believed to have formed the axial plane foliation S_1. No recognizable F_1 folds were seen in outcrop, however, some may exist in the banded quartz-magnetite iron formation. The S_1 foliation is not distinguishable from the S_2 foliation except in a few fold noses (Campbell, 1974). The S_1 foliation locally represents a syn-metamorphic fabric.

The second period of deformation, D_2, is believed to have caused a recognizable set of isoclinal folds which plunge shallowly southwest (242/009) (Campbell, 1974). These "F_2" folds crenulate the S_1 foliation and form a second axial plane foliation S_2, which is locally inclined to S_1. S_2 is biotite-rich and represents a second syn-metamorphic fabric (see Fig. 10). D_2 is also thought to have created the asymmetrical "Z" and "S" drag folds (F_2) mentioned previously, as well as the isoclinal chevron "kink" folds (F_2). The strain features F_2 and S_2 are most prominent in the paragneisses, although some isoclinal and drag folds are present in the iron formation.

The third, D_3, produced the warped axial planes of F_2. The F_3 folds are both major and minor tight isoclinal folds and trend northwest (Campbell, 1974). Beyond D_3 the deformation history becomes obscure but Campbell (1974) claims a fourth period of folding may be inferred as some folds seem to be refolded about a northeast trending axis.

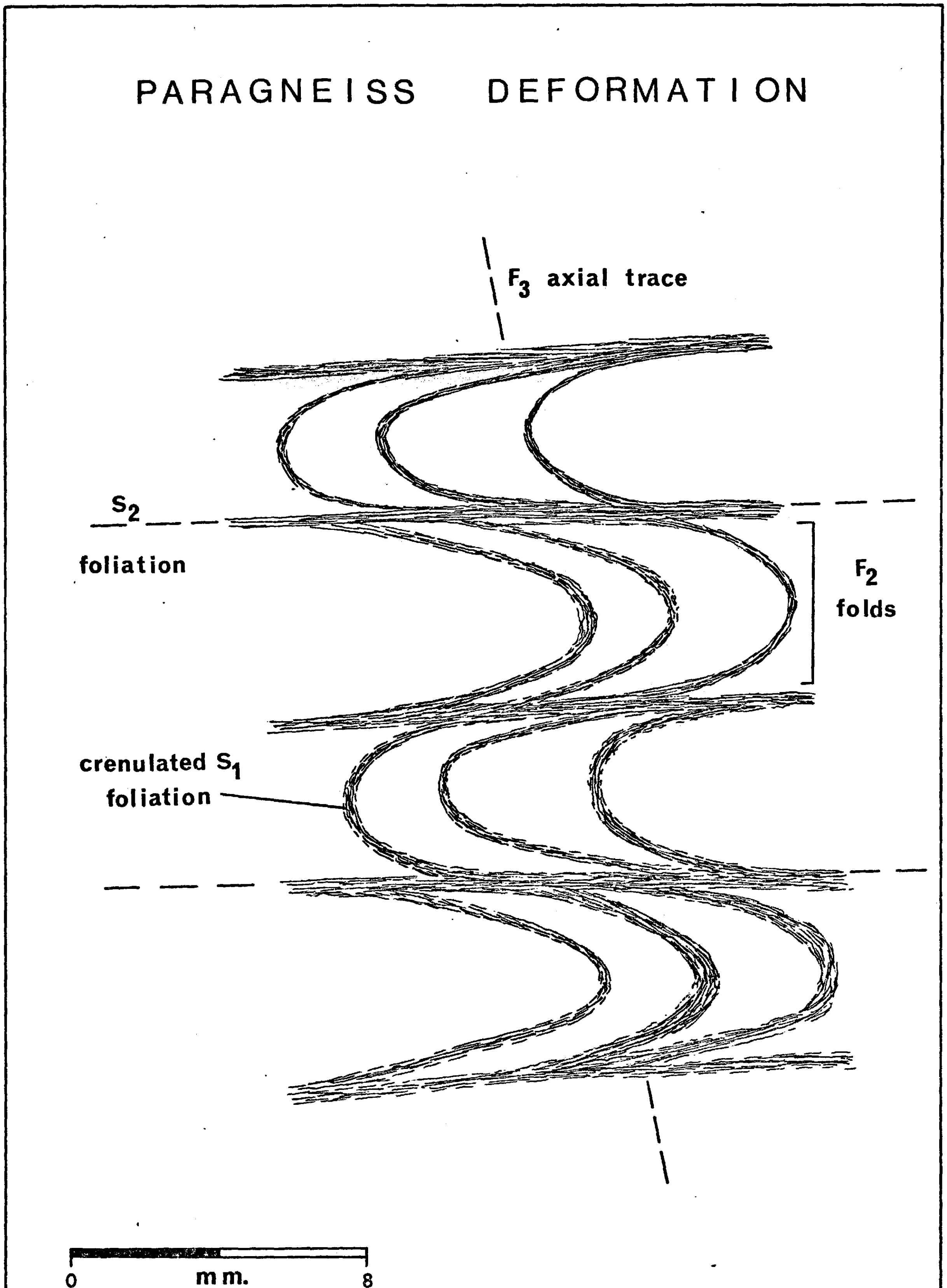
PARAGNEISS DEFORMATION
F3 axial trace
S2
foliation
F2
folds
crenulated S1
foliation
0
mm.
8
Scale

Fig. 10.

c) Faults, Dykes and Sills:

The study area is faulted into three major fault blocks by two northwest trending faults, A and B (see Fig. 4). The region to the east of fault B is displaced downwards with respect to the area west of the fault. Preliminary investigation has not disclosed any movement along fault A. Smaller faults with northwest trends occur locally. Small, pegmatite sills, and veinlets occur with the PAG greywacke sequence, mentioned above. The region is cut by northwest trending diabase dykes (also mentioned previously). Often these are discontinuous on the surface but are easily traced from the air. Prominent sills of granodioritic gneiss are found in the eastern part of the area and have been reported by Campbell (1974).

CHAPTER III

TEXTURES AND MINERALOGY

A petrographic study of a suite of selected rocks was undertaken. Both petrographic descriptions and accompanying sketches appear in Appendix A. The suite studied was composed of rocks from the various sequences of the PAG and included quartzites, greywacke-paragneisses, meta-ultrabasic rocks plus one sample of iron formation. The sample locations are plotted on Fig. 4, and UTM coordinates are listed along with the descriptions. The metamorphic minerals present are summarized in Table I.

i) Quartzite Sequence:

Samples examined from the quartzite sequence of the PAG were J73-006, -007 and -034. These samples are comprised of two mineral assemblages:

1) Quartz + Muscovite

2) Quartz + Muscovite + K-spar + Sillimanite (fibrolite).

Grain sizes of these rocks vary from 0.1 mm to 4.7 mm, and grains are generally anhedral. The sillimanite often occurs as fibrolite and is closely associated with the three phases quartz, K-feldspar and muscovite. These rocks show very little alteration and are extremely fresh. Any alteration which may have occurred is limited to strain effects and metamorphic mineral reactions.

TABLE I

MINERAL TALLY

Sample \ Mineral	QUARTZ	PLAGIOCLASE AB	PLAGIOCLASE AN	ORTHOCLASE	MICROCLINE	BIOTITE	MUSCOVITE	SERICITE	SILLIMANITE	HORNBLENDE	TREMOLITE	PYROXENE	ALMANDINE	CALCITE
Paragneiss														
J73-032	X	X		X		X	X	X	X					
J73-036	X		X	X	X	X	X	X						
J73-040	X		X	X	X	X	X	X						
J73-051	X		X	X		X							X	
J73-050-2	X		X	X		X							X	
J73-048	X		X	X		X	X	X	X					
J73-004	X	X		X		X				X				
J73-015	X		X	X		X		X		X			X	
J73-061	X		X	X	X	X	X	X	X					
Quartzite														
J73-006	X			X	X		X		X					
J73-007	X						X							
J73-034	X			X			X		X					
Meta-Amphibolite														
J73-055			X			X		X		X	X	X		X
J73-088	X		X			X				X	X	X		
Iron Formation														
J73-014	X			X						X		X		

Two notable effects of strain are the mechanical destruction of grain boundaries producing a "mélange" of intergranular anhedral quartz and orthoclase (sample J73-034), and the formation of unique ellipsoidal porphyroblasts of quartz and sillimanite-fibrolite (sample J73-006). The quartz grains are marginal and form a "crust" around the muscovite-sillimanite-fibrolite-rich nucleus. Crustal quartz grains are elongated and possess long axes parallel to that of the porphyroblast. Grain boundaries in this "crust" are smooth and continuous. Perhaps this represents partial recrystallization of grain boundaries contemporaneous with deformation. Two interesting trends displayed by the porphyroblast are confinement of muscovite-sillimanite-fibrolite to the nucleus and a definite decrease in K-feldspar as one moves from the groundmass towards the porphyroblast. An example of a quartz-muscovite-sillimanite-fibrolite porphyroblast is given in Figs. 11 and 12.

Metamorphic reactions which have occurred in this sequence are certainly limited. The most prominent reaction is the formation of sillimanite-fibrolite plus K-feldspar (orthoclase) from quartz and muscovite. Evidence of this reaction is present in the nucleus of the porphyroblasts of sample J73-006, and in the small porphyroblasts of J73-034. In the latter case the sillimanite occurs as wisps radiating from the porphyroblast. Both of these examples indicate sillimanite-fibrolite growth under anisotropic conditions associated with late stage deformation. Also the fact that none of the sillimanite-fibrolite exhibits any relict textures supports the late-stage formation of this

Figure 11. A thin section print of a sillimanite-fibrolite porphyroblast from sample J73-061. Note the sillimanitic nucleus surrounded by a quartz-rich crust. The orientation of these grains parallels the long axis of the porphyroblast. The magnification is 5X and is taken under X-nicols.

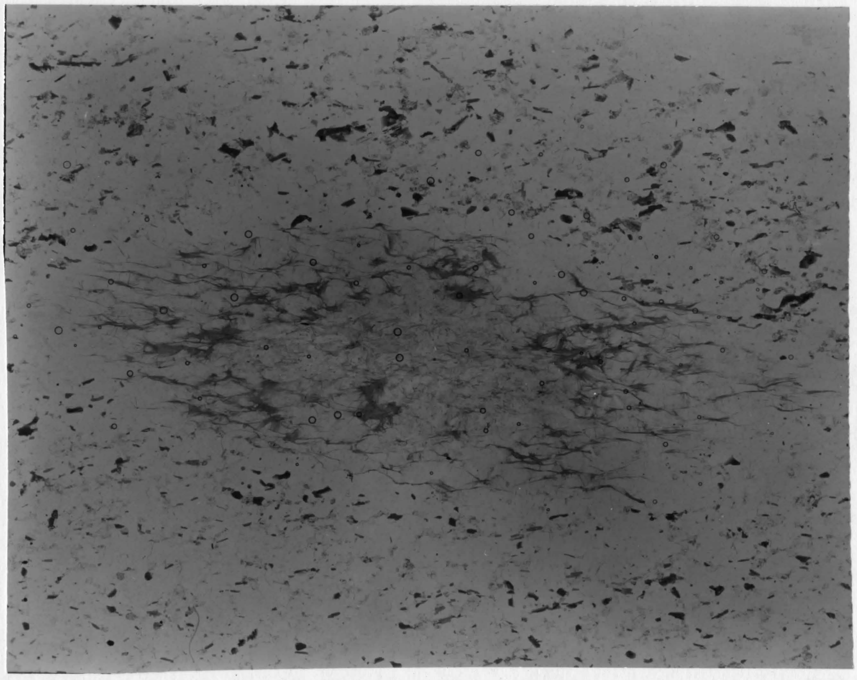

Figure 12. The same thin section print but taken under plane polarized light shows the biotite foliation and the quartz halo around the porphyroblast.

mineral (see Figs. 13 and 14).

Another reaction associated with metamorphism may be the formation of fuchsite. This chromium version of muscovite could have quite easily formed during late stage metamorphism when chromium ions were mobile and accepted by the sheet silicates. It is difficult to say whether ion migration was directly from nearby amphibolites or from detrital chromium.

Deformation of the quartzites is indeed minor with respect to other members of the PAG. This combined with the freshness of the rock, relative purity of silica-rich minerals and a lack of metamorphism strengthens field data suggesting it to be the youngest member of the PAG.

The quartzite sequence contains a minor greywacke unit which may be a lateral facies change (mentioned above). Sample J73-061 is an example of this quartzite-associated greywacke. The main mineralogical differences between this rock and the quartzites is an increase in K-feldspar content, the presence of plagioclase, biotite and a mafic oxide plus detrital tourmaline. The biotite grains define the foliation and sillimanite-fibrolite-quartz porphyroblasts are very similar structurally and mineralogically to those found in the quartzites. This indicates that the same deformation event caused the formation of sillimanite-quartz porphyroblasts in both facies of this sequence. The biotite foliation is probably contemporaneous with this deformation. Little alteration is apparent but feldspars are altered to sericite along both cleavage and twin planes. Sillimanite-fibrolite growth has occurred under the influence

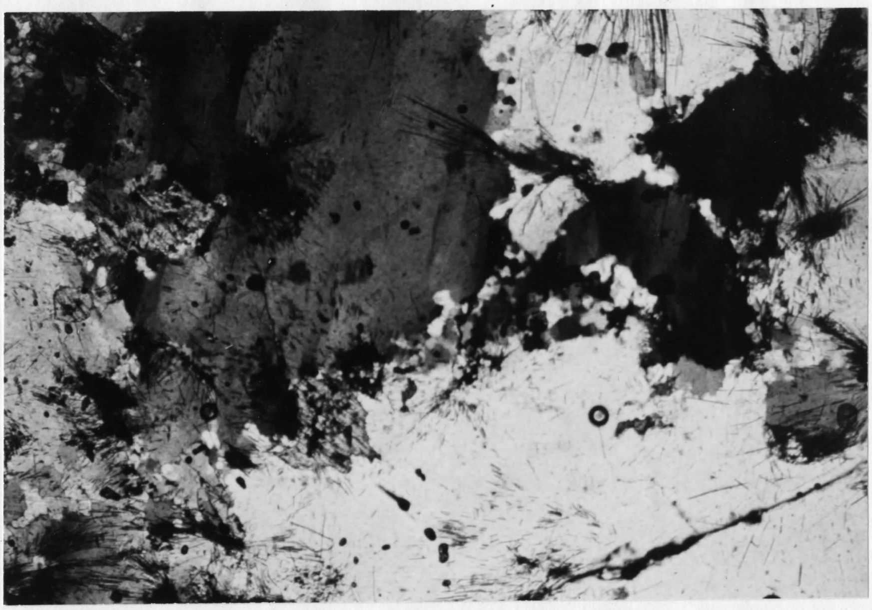

Figure 13. Taken from sample J73-032 this photomicrograph shows the dehydration reaction of muscovite. To the lower left of centre is a small muscovite grain which has an extinguished quartz grain above it and one which is not below it. The muscovite is anhedral and poikilitic with inclusions of quartz and K-spar. Magnification is 45X.

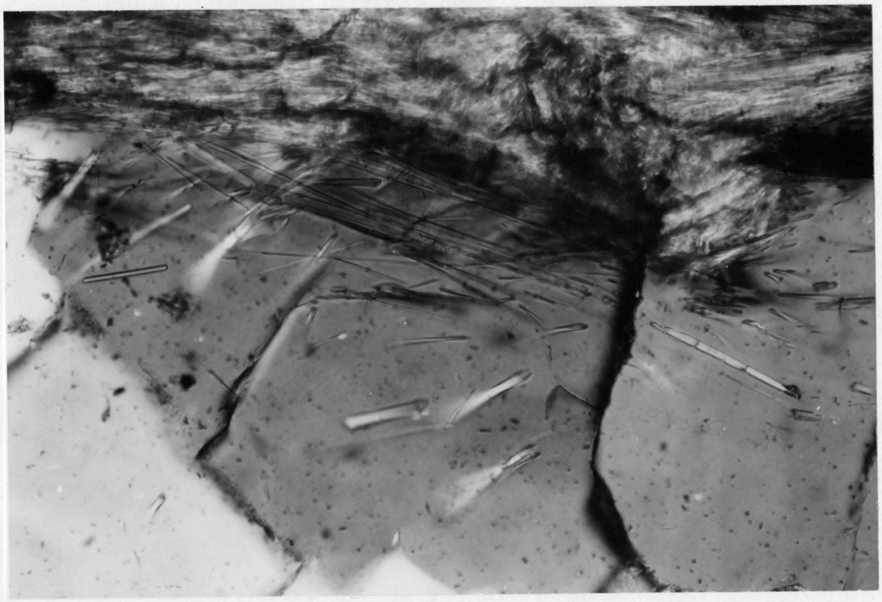

Figure 14. Taken from sample J73-048 this photomicrograph shows matted fibrolite along the upper edge, discrete fibrolite grains in upper centre, and quartz grains in the lower portions. Magnification is 400X.

of an anisotropic stress field which may be contemporaneous with porphyroblast formation. Sample J73-061 is listed under the paragneiss heading in the mineral tally (see Table 1).

ii) Greywacke-Paragneiss Sequence:

The greywacke-paragneiss sequence of the PAG includes quartzo-feldspathic biotite greywacke-paragneiss samples J73-032, -036, -040, -051, -050-2, -048, -004, and -015, plus iron formation sample J73-014. The paragneiss-greywackes can be divided into three groups, those containing muscovite, almandine garnet, and hornblende. The respective mineral assemblages characteristic of these groups are:

1) Quartz + Plagioclase + K-spar + Biotite + Muscovite ± Sillimanite (fibrolite)

2) Quartz + Plagioclase + K-spar + Biotite + Almandine Garnet

3) Quartz + Plagioclase + K-spar + Biotite + Hornblende ± Almandine Garnet.

Unlike the quartzites, the greywacke-paragneiss rocks show much deformation and mineral alteration is more common.

a) Muscovite-bearing Paragneisses:

Samples of the first group are J73-032, -036, -040 and -048. In each of these samples the phases quartz, plagioclase, K-feldspar and biotite combine to form at least 80% of the rock by volume. Muscovite is present varying from 1% to 15%. Those samples with muscovite over 5% also contain sillimanite. The sillimanite-fibrolite varies from 4%

to 12% and is closely associated with quartz, muscovite and K-feldspar (samples J73-032 and -048).

Deformation in this group is best defined by the mica foliation which is comprised of both the phases muscovite and biotite. Sample J73-032 displays parallel to sub-parallel sets of biotite and muscovite blades which show a definite inclination to the prominent foliation. These may be indicative of an earlier (S_1) foliation. Also present in this sample are sillimanitic porphyroblasts with radiating wisps (see Fig. 13) indicative of growth in an anisotropic stress field (D_3). The prominent biotite foliation is probably S_2. Sample J73-048 shows another strain phenomenon, "en echelon" isoclinal folds. These are very tight folds (see Figs. 10 and 15). When muscovite occurs in the fold nose it has often reacted with quartz to give sillimanite and K-feldspar. This sillimanite shows no relict textures and no preferred orientation. Its growth is isotropic and may be associated with M_3. This hypothesis suggests that little sillimanite formed during D_2 but that the stored strain energy imparted to the muscovite grains, as a result of D_2, was augmented by the thermal energy of M_3 triggering the reaction between muscovite and quartz. Metamorphic differentiation is present in the continuous S_2 biotite foliation and the isoclinal folds define crenulated S_1 foliations (see Fig. 15).

Mineral reactions include the above reaction producing sillimanite but mineral alteration is omnipresent. Sericitization of the feldspars is always found and often oxidation of biotite grains produces

Figure 15. Taken from sample J73-048 this photomicrograph shows tight microscopic isoclinal folding of the S_1 foliation. The continuous extinguished biotites paralleling the edges of the micrograph represent the S_2 foliation. In some fold noses dark "cloudy" areas are found. These represent fibrolitic regions formed from the dehydration of muscovite. Note that muscovite grains in the fold limbs are not altered. Separating the biotite layers are quartzo-feldspathic layers. Magnification is 45X.

a mafic oxide, which is, at least in part, magnetite. Tourmaline (schorlite) is also found and appears unaltered, but fractured. Perhaps this is a detrital mineral which has survived metamorphism, acting as a chemical and kinetic inert phase. Zircon is omnipresent and limited to biotite grains.

b) Almandine Garnet-bearing Paragneisses:

Samples of this group are J73-051 and -050-2. In these rocks the phases quartz, plagioclase, K-feldspar and biotite combine to form over 90% of the rock. Almandine garnet varies in abundance from 3% to 7%. In outcrop these rocks occur very close to iron formations, and locally may grade into these rocks. The most striking feature of these samples is not only the presence of almandine garnet but its metamorphic and tectonic relationships.

The most prominent deformation feature of the almandine garnet paragneisses is the foliation defined by the biotite-rich layers. This is probably a S_2 foliation. Some biotites inclined to this foliation may be reminiscent of an earlier S_1 foliation. Both samples are from the T-bar Lake section (see Fig. 4), and are cut orthogonally to each other to display both cross-sectional and linear aspects of the deformation. The cross-sectional plane shows that the foliation is "kinked" on a minute scale. This kinking may be due to stresses associated with late D_2. The almandine garnet poikiloblasts are fractured and contain inclusions of mafic oxide, biotite, quartz, and K-feldspar. The last two are found in parallel to sub-parallel trains and are probably a relict form of the S_1 foliation. No rotational growth structures are found in the garnets indicating garnet growth occurred after D_1, and before D_2. Rotation took place in the early stages of D_2, before the formation of the S_2 biotite foliation which wraps the garnet (see Figs. 16 and 17).

Associated with these garnet porphyroblasts are pressure shadows filled with quartz and K-feldspar. These grains are larger than their counterparts elsewhere in the section and possess sutured grain boundaries. These pressure shadows were created after rotation of the garnet during D_2. The sutured nature of the sialic material can be associated with early D_2 deformation of M_1 compositional layering as these shadows escape any deformation accompanying the formation of the enclosing foliation. Similarly the undulose extinction found in these grains is probably a result of straining associated with early D_2.

The principal mineral reaction in these samples is the formation of almandine garnet. It is difficult to determine which reaction was involved but the source of iron was, at least in part, from biotites associated with metamorphic event M_1. Iron migration may have been influenced by nearby iron formations. Little alteration of these rocks has occurred but minor oxidation of biotite can be found.

c) Hornblende-bearing Paragneisses:

The samples of this rock type are J73-015 and -004. In these samples the phases quartz, plagioclase, K-feldspar, biotite and hornblende combine to form 88% to 97% of the rock. Hornblende comprises 29% to 62%

Figure 16. Taken under X-nicols from sample J73-050-2 this photomicrograph shows a rotated garnet poikiloblast. The garnet is almandine and is completely extinguished. The parallel trains of anhedral sialic inclusions in the garnet are reminiscent of the S_1 foliation. The S_2 biotite foliation wraps the poikiloblast as can be seen in the right portion of the photomicrograph. Magnification is 45X.

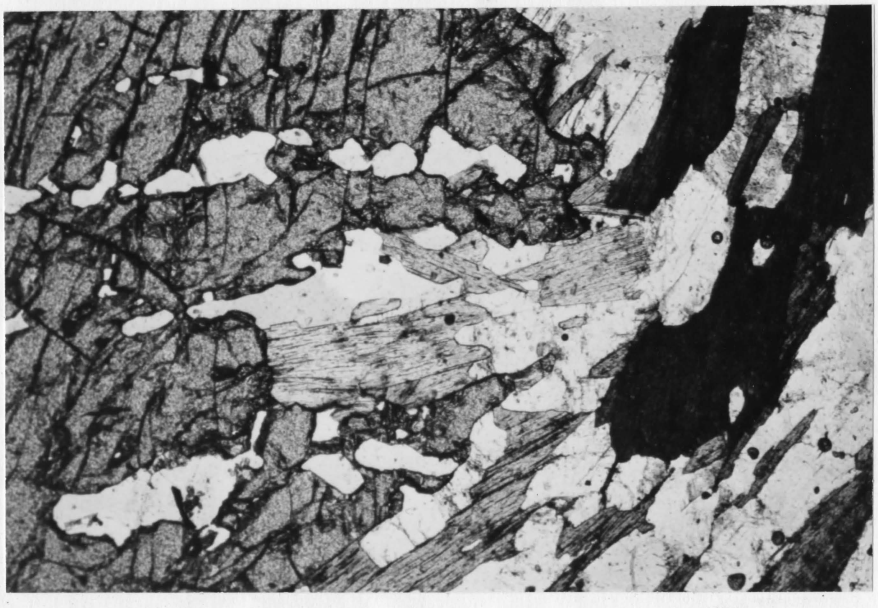

Figure 17. The same photomicrograph as above but taken under plane polarized light readily highlights the fractures in the almandine garnet.

of the samples. The foliation-gneissosity is defined by the hornblende-biotite-rich layers. In sample J73-004 these are kink-folded forming "en echelon kinks". This may be an S_2 foliation. Biotite and hornblende grains inclined to this foliation may be remnants of an S_1 foliation. Fold limbs are deformed around hornblendes whose long axes are orthogonal to the principal foliation. Such hornblendes represent a more competent perturbation simply because of their orientation.

Sample J73-015 shows the textural relationship between almandine garnet and hornblende. This relationship is analogous to the garnet-biotite relationship mentioned above. The garnet shows inclusions of quartz, K-feldspar, and hornblende, and is highly fractured. However, the garnet is not rotated. The prominent foliation present is an S_2 foliation with garnet assimilation probably occurring after the formation of S_1 foliation, but during M_1. The invasion of quartz along cleavage planes in the biotites indicates these may be relicts of an S_1 foliation.

Mineral reactions occurring in these samples are essentially confined to the formation of garnet and various alteration phenomena. Iron for the formation of garnet may have come from the hornblende and to a lesser extent the biotites, but the nearby iron formation should not be disregarded as a potential donor. Alteration in these samples includes formation of a brown mafic oxide from the garnet, and a black mafic oxide from some hornblendes and biotites. Plagioclase grains may show slight sericitization. The protolith for the hornblende present is the meta-amphibolite rocks which are spatially closely associated with the hornblende paragneisses.

d) Iron Formation:

The only sample of iron formation examined was J73-014. This is a banded quartz-magnetite iron formation with minor hornblende and pyroxene. As was mentioned earlier another iron formation exists and is composed of the two phases quartz, and magnetite. The iron formation examined in this study was associated with the hornblende paragneiss J73-015 and some meta-amphibolites. The iron formation shows a well defined gneissosity. Alteration is minor but some hornblende grains may be corroded to a brown mafic mineral. Study of the iron formation was not intensive but included for completeness.

iii) Meta-Ultrabasic Rocks:

Meta-ultrabasic samples include J73-055 and -088. These samples contain 62% to 86% amphibole and 5% to 10% biotite, but less than 1% plagioclase. The amphiboles present are hornblende and tremolite. Sample J73-088 has extremely long (up to 22 mm) tremolite blades which define the foliation present, but J73-055 shows no preferred orientation of the fabric. Biotite occurs in both rock types but is by no means genetically similar. In J73-088 some of the biotite grains are formed by alteration of the hornblende present, as is portrayed by the presence of highly altered hornblende inclusions in the poikilitic biotite grains. In sample J73-055, however, the biotite grains are not deformed or corroded and show no relict textures. These latter biotites probably have a sedimentary origin. The presence of tourmaline (schorlite) in this sample is further evidence of a sedimentary history for the rock, as it is definitely a detrital mineral. Calcite and siderite were also found in this rock, and tend to be alteration products from calcium-plagioclase, plus any iron-bearing phases present. Pyroxene is also found in these rocks but in amounts less than 5%.

In summary, the greywacke-paragneiss sequence contains a great wealth of information concerning the metamorphism and deformation of the PAG. This material is supplemented by the quartzite sequence which withholds much of the late deformational and metamorphic history, without the guise of earlier events. The meta-ultrabasic rocks of the group also contribute to the cause, but to a lesser extent.

CHAPTER IV

PETROCHEMISTRY

i) Analytical and Data Reduction Methods:

Whole rock analyses of samples from the quartzite sequence, greywacke-paragneiss sequence and meta-ultrabasic rocks were obtained using X-ray fluorescence. The slab left over from thin-sectioning was crushed to 200 mesh using a shatter box with tungsten-carbide rings. These slabs were most convenient as they possessed no weathered surfaces, provided 10 grams or more of crushed sample and gave chemical analysis for a portion of the rock not much different than the thin section studied.

Pressed discs of each sample were made following the procedure outlined by Marchand (1973). These discs of boric acid and sample were then analysed on a Philips automatic sequential spectrometer, model PW1450, at McMaster University. The spectrometer is programmed to analyse four different samples for 10 major elements in each run, which takes from 10 to 15 minutes. The major elements analysed include Si, Al, total Fe, Mg, Ca, Na, K, Ti, Mn, and P. A chromium discharge tube was used throughout the entire analysis.

In order to obtain a handle on machine variance during the testing period one sample remained in the spectrometer at all times acting as a drift monitor. Forty-nine standards were run with the rocks being analysed. The standards included basic volcanics, high alumina rocks and a SiO_2 disc, in order that a complete range of concentrations would be available for data reduction.

The data reduction method used to obtain weight percent oxides from counts per time interval was taken from Brown et al. (1973). The unnormalized whole rock analysis in weight percent oxides appears in Appendix B, and normalized values are presented in Table II.

The plotting of various binary and ternary chemographic diagrams was achieved through computer techniques. Modification of B. M. Gunn's program Triang was achieved by the present author. The modified version, Trimod, includes the plots from the original Triang program plus the ternary plots Al_2O_3-K_2O-Na_2O, AFM projection through muscovite, and an ACF plot. A copy of program Trimod is found in Appendix C. In the program, columns 73-80 contain a sequential code. The first three columns contain either the alphanumerics PLT or WLF. Those possessing the code WLF are additions made by the writer. Column 76 is blank and columns 77-80 possess the numeric ordering of the cards. Interjections by the writer include an alphanumeric prefix in columns 78 or 79 and are to be used for alphabetic ordering of these cards.

TABLE II

WHOLE ROCK ANALYSIS

IN

WEIGHT % OXIDES (NORMALIZED)

Samples	SiO_2	Al_2O_3	Fe (total)	MgO	CaO	NaO	K_2O	TiO_2	MnO	P_2O_5
Greywacke-Paragneiss										
J73-032	77.31	12.21	4.21	1.70	1.47	0.35	2.26	0.36	0.05	0.09
-036	66.40	16.60	4.48	1.92	2.58	4.61	2.62	0.58	0.06	0.14
-040	85.52	7.96	1.92	0.62	2.51	0.35	0.91	0.15	0.02	0.04
-051	63.88	15.32	7.21	4.09	2.51	3.46	2.59	0.73	0.10	0.12
-050-2	62.62	15.12	9.29	3.69	1.91	3.48	2.97	0.68	0.20	0.04
-048	59.70	17.65	9.00	4.85	1.36	1.89	4.59	0.80	0.09	0.07
-004	53.50	8.96	15.34	10.70	6.59	0.33	3.30	0.82	0.22	0.24
-015	50.49	9.37	25.19	3.87	7.97	1.19	0.78	0.53	0.46	0.14

Continued.........

TABLE II -- Continued

Quartzite										
J73-006	90.86	5.91	0.28	0.05	0.04	0.22	2.56	0.06	0.01	0.02
-007	94.41	6.06	0.34	0.07	0.04	0.20	2.79	0.06	0.01	0.02
-034	90.52	9.05	0.24	0.03	0.02	0.02	0.07	0.03	0.01	0.01
Meta-Ultra-basic										
J73-055	49.60	10.62	14.25	12.41	10.47	0.44	1.43	0.47	0.24	0.08
-088	50.94	8.21	17.57	15.37	6.11	0.75	0.26	0.46	0.25	0.07

ii) Chemographic Plots:

a) Al_2O_3-Na_2O-K_2O Plot:

Since in pelitic rocks all compositions plot above the boundary defined by 50% Al_2O_3, only the top half of this plot is shown (see Fig. 18). Both samples plotted contain the coexisting phases sillimanite, muscovite, orthoclase, quartz and biotite. Plagioclase can exist with these as is evident from the petrography. This phenomenon can be explained by the fact that plagioclase has a Ca, or anorthitic member. Since most plagioclases in the PAG studied above were intermediate in composition the Ca member has a prominent role in the topology of this plot. By adding the fourth component, Ca, the system becomes quaternary and the sillimanite-orthoclase tie line can be crossed allowing the coexistence of a calcic plagioclase with the above mineral assemblage.

b) AFM Plot:

Illustrated in Figure 19, this plot shows the clear distinction between sillimanite-rich rocks and the biotite-rich ones, or the quartzitic rocks and the greywacke-paragneisses. Only samples containing muscovite and quartz can be plotted on this projection, hence, those containing almandine are absent. Since biotite is present in the paragneisses in large amounts, the mafic member of this plot has a great effect in pulling the bulk composition away from the alumina vertex.

Fig. 18 .

Al2O3-K2O-Na2O PLOT

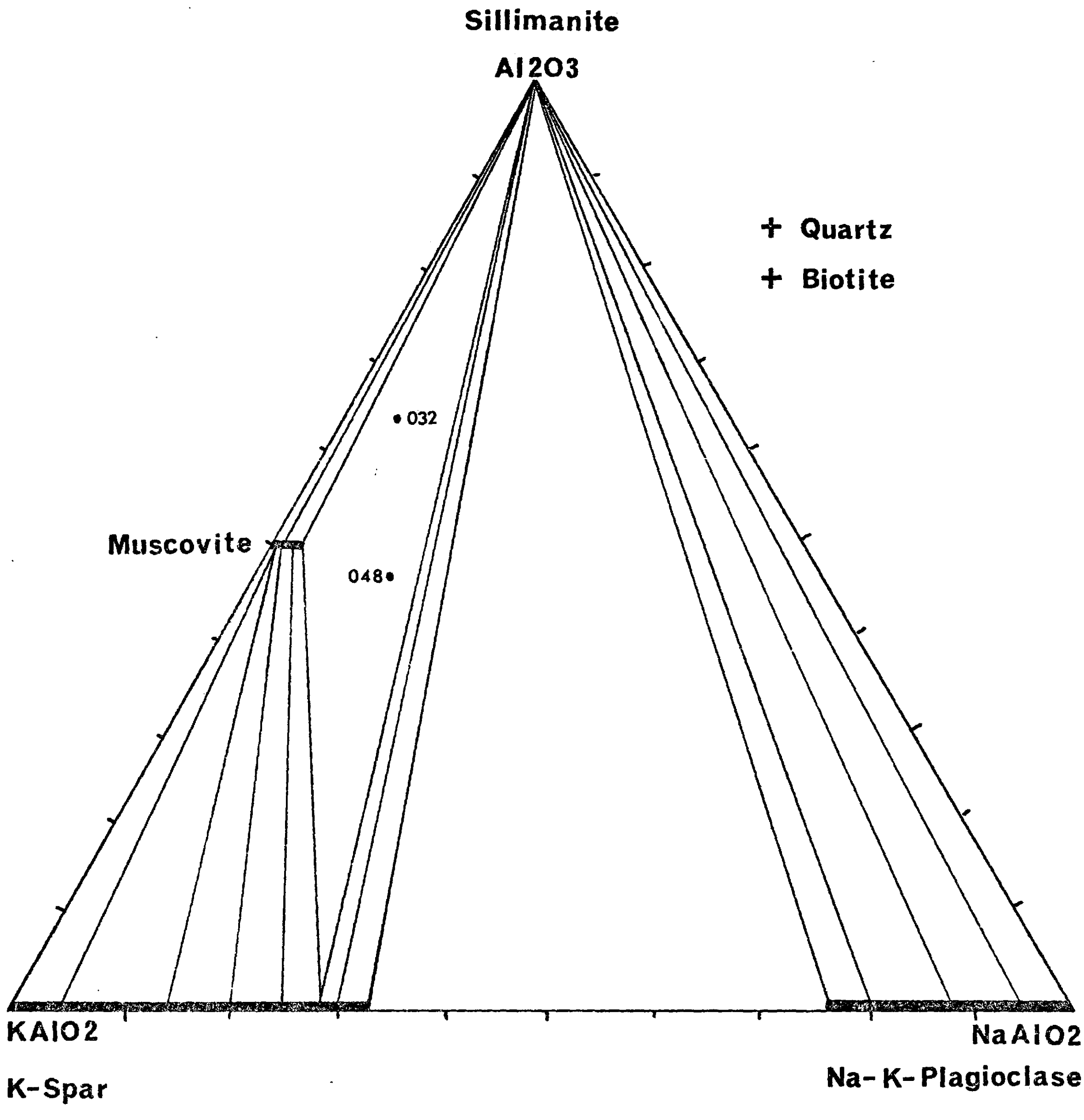

Fig. 19 .

AFM PLOT

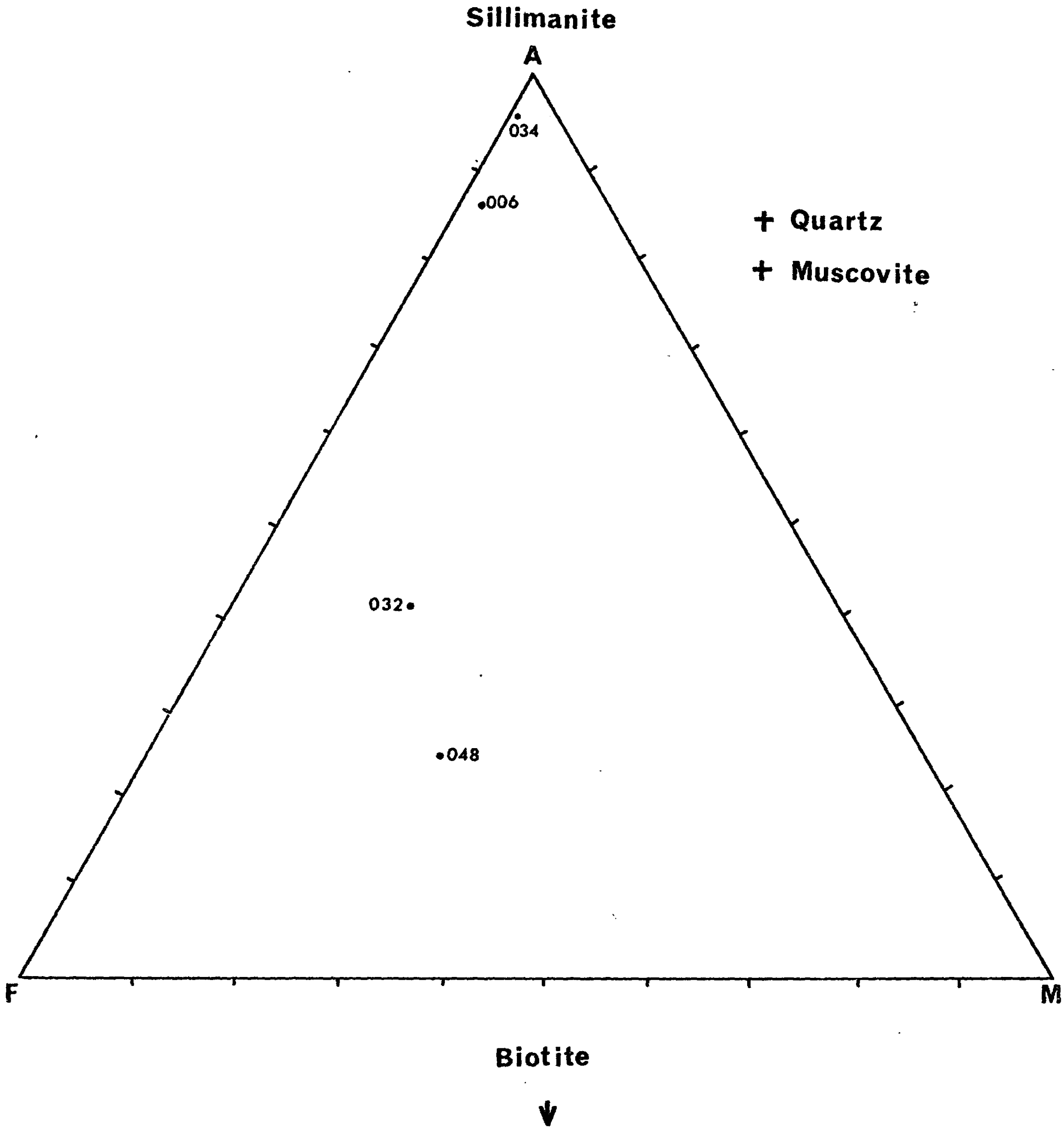

c) ACF Plot:

The ACF plot is shown in Figure 20 and shows that three general groupings exist. The first is a family of three clustered near the alumina apex. The second a cluster of six above and to the right of the upper boundary of the hornblende field. Lastly, the third group has three members near the mafic apex.

The first family are quartzites and contain very little mafics or calcium but sillimanite is present causing a relative enrichment in alumina in this plot.

The second family show two possible sets of mineral assemblages, one containing sillimanite, almandine, and anorthitic plagioclase, and the other almandine, anorthitic plagioclase and hornblende. Neither of these assemblages are observed in PAG rocks. This can be explained by the strong influence of K due to the presence of biotite. The potassium component will tend to pull the compositions out of this projection and into the volume created by the ACFK tetrahedron. Since biotite is the prominent potassium-bearing mineral, compositions would be biased towards the biotite field. This may be shown graphically by an ACFK plot, but unless a true stereoscopic tetrahedron is used, the effectiveness is lost.

The third family of points represents hornblende-bearing assemblages. With the exception of J73-004 these have very little biotite, hence, their plotted positions are acceptable. Because of the influence of biotite, sample J73-004 will be transposed into the volume created by the ACFK tetrahedron similar to that mentioned above. However, this plot

Fig. 20.

ACF PLOT

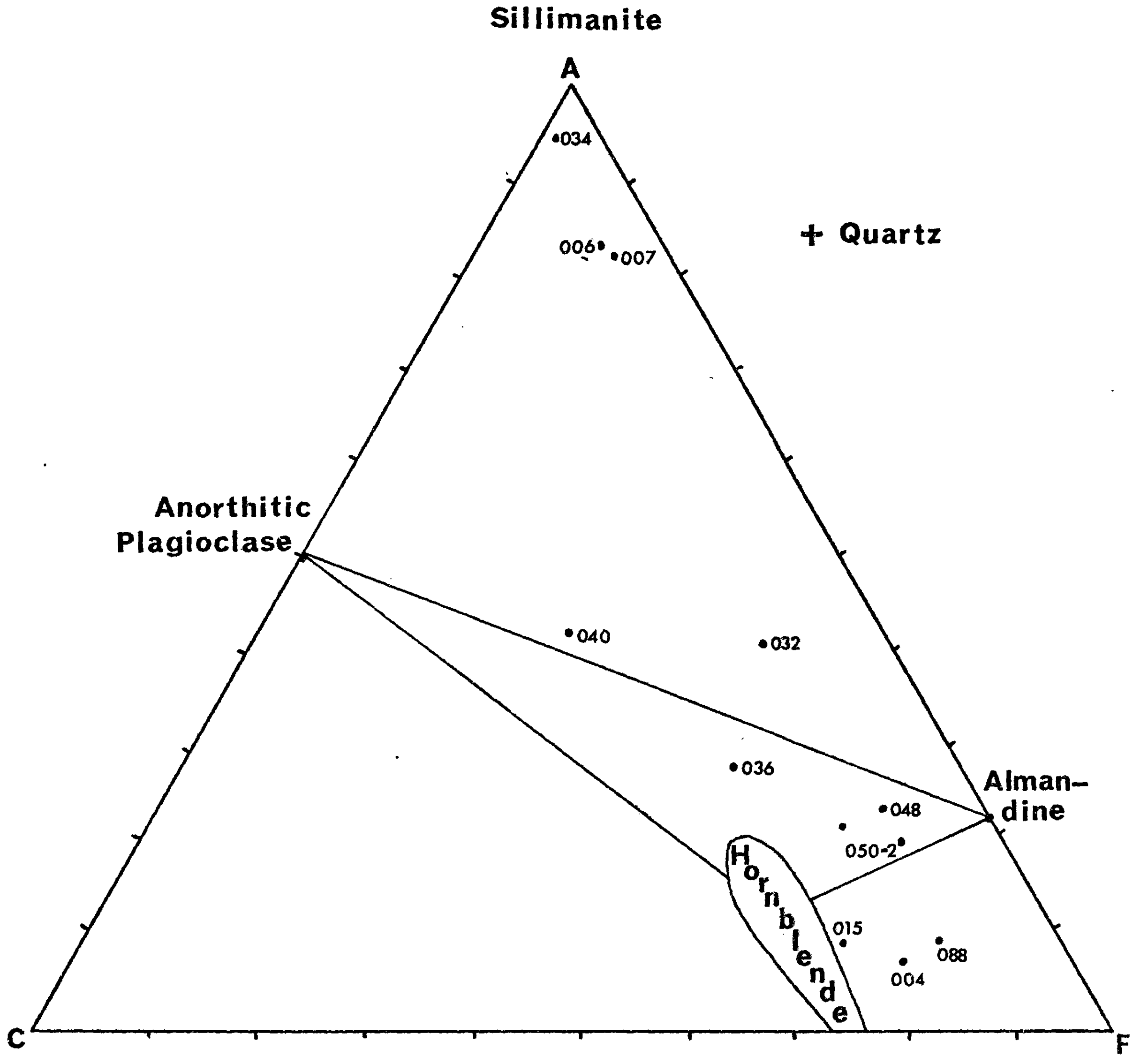

does indicate that the amphiboles present lie outside the hornblende field, thus, the amount of Mg in these minerals is substantial.

The ACF plot also shows that the samples are rich in mafics and alumina but poor in calcium.

iii) Chemical Evidence of PAG Protoliths:

Examination of the whole rock analyses, Table II, indicates that both miogeosynclinal and eugeosynclinal facies are present in the PAG. The miogeosynclinal facies is characterized by the quartzite sequence. Chemically, this sequence has very high SiO_2 values, low Al_2O_3 concentrations, and a MgO/CaO ratio which can be as high as 3 (see Fig. 21).

The eugeosynclinal facies is typified by the greywacke-paragneiss sequence. SiO_2 values are substantially lower than the quartzite sequence and Al_2O_3 values are much higher. These are indicative of a high degree of detritus. The MgO/CaO ratio for this sequence is biomodal having values both higher and lower than 1 (see Fig. 21). Such a distribution suggests that both eugeosynclinal, and miogeosynclinal facies are present in this sequence. Perhaps this sequence progressed from a eugeosynclinal setting to a miogeosynclinal setting climaxed by the deposition of the quartzite sequence.

The meta-ultrabasic rocks are chemically similar to basalts. These probably represent a volcanic introduction into the group.

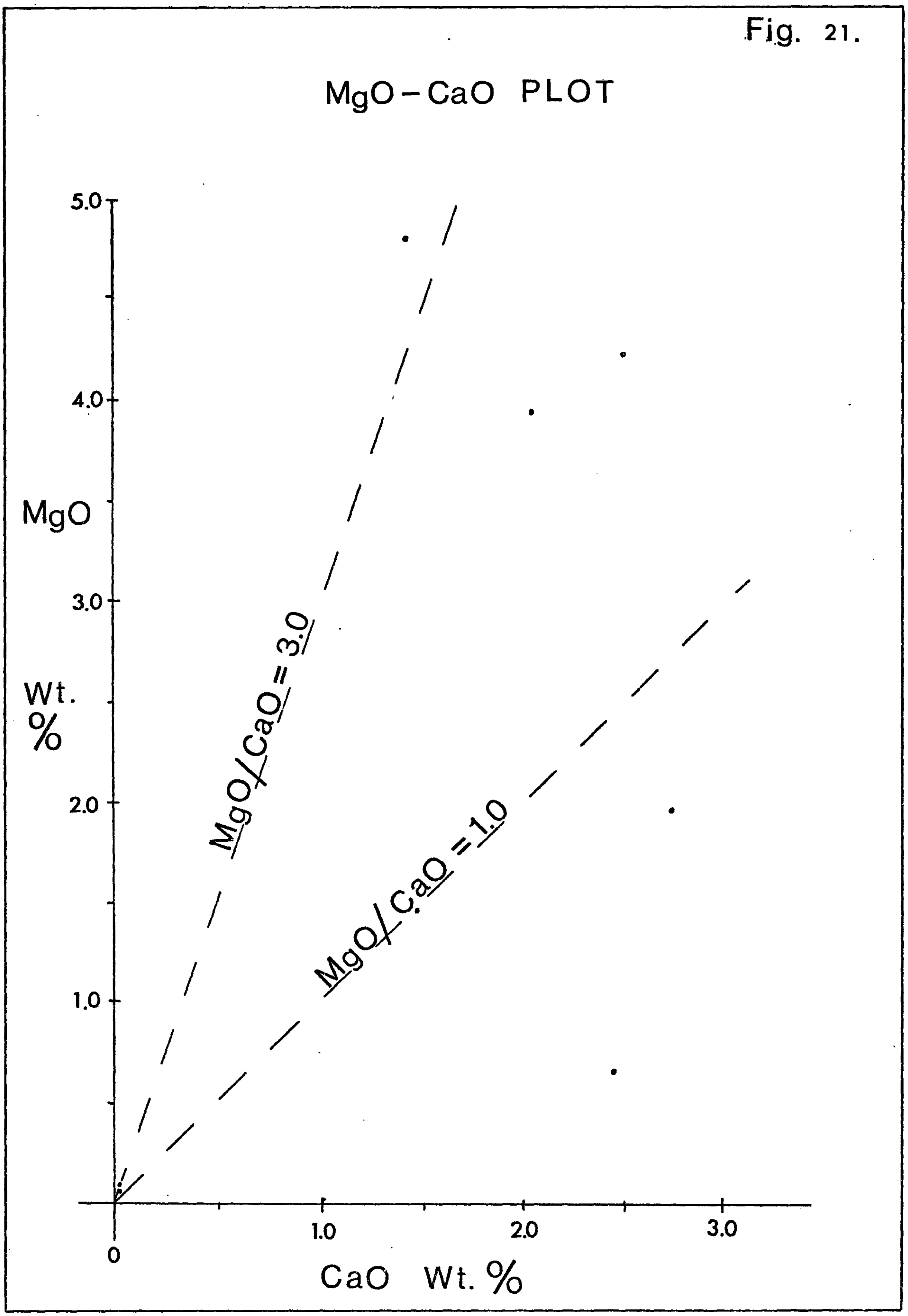
Fig. 21.
MgO - CaO PLOT
MgO
Wt.
%
5.0
4.0
3.0
2.0
1.0
0
1.0
2.0
3.0
CaO Wt. %
MgO/CaO = 3.0
MgO/CaO = 1.0

Protoliths for the quartzite sequence may be quartz sandstone with clay-rich layers (illustrated today by sillimanitic portions). The greywacke-paragneiss sequence probably stemmed from greywackes, interspersed with layered iron formations. Lastly, the present-day meta-ultrabasic rocks stem from basaltic lavas.

CHAPTER V

METAMORPHISM

Metamorphism in the PAG can be considered on two major levels, regional and local. Results of examination of these two should allow conclusions to be made concerning the pressure and temperature regime of metamorphism; the structural and chemical influences; time relations between metamorphic events, and possible contributions towards the construction of an orogenic model.

i) Regional Grade of Metamorphism of the PAG:

The regional grade of metamorphism for the PAG was stated by Frisch (1973) to be of the amphibolite grade both within the PAG and in orthogneisses outside of the group. This conclusion was made from data gathered to the east, south, and west of Committee Bay. This metamorphic grade is substantiated by the occurrence of sillimanite plus some kyanite to the west, Schau (1974).

ii) Metamorphism of the PAG-Ellice Hills Sheet:

From the mineral assemblages found both in thin section and hand specimen the PAG rocks in the study area are definitely of the Almandine-amphibolite grade of metamorphism as defined by Winkler (1967). In fact, the rocks of the PAG are distinctly members of the Sillimanite-orthoclase-almandine Subfacies (B 2.3, Winkler, 1967) of Barrovian type regional metamorphism.

a) Mineral Assemblages Present:

Membership in this subfacies is apparent from the following mineral assemblages present:

from the quartzite sequence:

Quartz + Muscovite + K-spar + Sillimanite (fibrolite)

from the greywacke-paragneiss sequence:

Quartz + Plagioclase + K-spar + Biotite + Muscovite ± Sillimanite (fibrolite)

Quartz + Plagioclase + K-spar + Biotite + Almandine Garnet

Quartz + Plagioclase + K-spar + Biotite + Hornblende ± Garnet

from the meta-ultrabasic rocks:

Hornblende + Tremolite + Biotite + Plagioclase ± Diopside.

The important mineral relationships to note are the coexistence of sillimanite and orthoclase, plus, the coexistence of almandine garnet and orthoclase, both in the absence of kyanite. Also, the presence of the amphiboles hornblende and tremolite in the presence of a calcic plagioclase yet in the absence of any epidote in the ultrabasic rocks is indicative of this subfacies. Coexistence of almandine garnet and hornblende in the absence of epidote is another assemblage present which is characteristic of this subfacies. It must not be forgotten that biotite is essentially omnipresent in the above rocks, with the exception of some members of the quartzite sequence. This point will be discussed below. Plagioclase contents for the rocks tend to be calcic ranging from An_{45} to An_{68}, with most falling in the labradorite field between An_{50} and An_{60}. A reason for these intermediate An values may be that some of the sodium from the plagioclase is being taken into the K-feldspar solid solution series between the end members orthoclase and microcline. This can be justified by the fact that K-feldspar to total feldspar ratios for the greywacke-paragneiss rocks are high (ranging from 0.7 to 0.8), and by the presence of the more sodic end member, microcline, in several specimens.

The lack of certain minerals in some rocks must be explained. These do not necessarily represent rocks of a different metamorphic grade, but are simply rocks whose chemical composition was such that various minerals could not form. For instance all samples which contain sillimanite in this suite also contain muscovite and quartz. Others contain no muscovite, but almandine, biotite and quartz are present, and yet others are chiefly composed of amphibole and biotite. Besides chemical limitations kinetic influences also determine which minerals or mineral groups are formed.

b) Metamorphic Mineral Reactions Present:

Metamorphic mineral reactions which may have taken place in the PAG rocks appear to be few and simple. The first and most prominent is the formation of sillimanite-fibrolite. Petrographic observation of this reaction clearly points out that sillimanite-fibrolite and orthoclase formed at the expense of quartz and muscovite (see Fig. 13). The most probable reaction for this event is the following, after Guidotti (1963).

$$\underset{\text{muscovite}}{KAl_2AlSi_3O_{10}(OH)_2} + \underset{\text{quartz}}{SiO_2} \rightleftharpoons \underset{\text{orthoclase}}{KAlSi_3O_8} + \underset{\substack{\text{sillimanite}\\\text{(fibrolite)}}}{Al_2SiO_5} + \underset{\text{water}}{H_2O} \quad (1)$$

This is the simplest reaction by which sillimanite can be formed from these reactants. Another reaction which should be considered is similar but involves the albite component of plagioclase.

$$\underset{\text{muscovite}}{K_{.94}Na_{.06}Al_2AlSi_3O_{10}(OH)_2} + \underset{\text{quartz}}{SiO_2} + \underset{\substack{\text{albite component}\\\text{of plagioclase}}}{0.1NaAlSi_3O_8} \rightleftharpoons$$

$$\underset{\text{orthoclase}}{1.1(K_{.86}Na_{.14}AlSi_3O_8)} + \underset{\substack{\text{sillimanite}\\\text{(fibrolite)}}}{Al_2SiO_5} + \underset{\text{water}}{H_2O} \quad (2)$$

It is clear that this reaction uses very little albite and it would be expected that some would remain after the reaction had taken place. However, had both quartz and muscovite been in excess (as they are), and the albite component of plagioclase was minor, it may have been totally exhausted in the formation of sillimanite, orthoclase and water. If this reaction is applicable to the PAG it could not be used to describe the formation of sillimanite in the quartzites as no plagioclase is present.

A third reaction which must be considered involves the paragonite component of muscovite.

$$NaAl_2AlSi_3O_{10}(OH)_2 + SiO_2 \rightleftharpoons NaAlSi_3O_8 + Al_2SiO_5 + H_2O \quad (3)$$

paragonite component of muscovite	quartz	albite component of plagioclase	sillimanite (fibrolite)	water

The total amount of paragonite component which can exist at this grade of metamorphism is equal to one-third of the muscovite component present (see chemographic plot of Al_2O_3-K_2O-Na_2O, Fig. 18). Even so, it is not likely that this is a valid reaction for the PAG as no albite component of plagioclase is found.

Another mineral reaction which applies to these rocks is the formation of almandine garnet plus orthoclase and water from muscovite, biotite and quartz (after Winkler, 1967).

$$KAl_2Si_3AlO_{10}(OH)_2 + K(MgFe)_3Si_3AlO_{10}(OH)_2 + 3SiO_2 \rightleftharpoons$$

muscovite — biotite — quartz

$$(MgFe)_3Al_2Si_3O_{12} + 2KAlSi_3O_8 + 2H_2O \quad (4)$$

almandine garnet — orthoclase — water

This reaction yields twice as many moles almandine garnet as muscovite used. The garnet produced is not 100% almandine but has a pyrope component equal to the Mg/Fe ratio of the biotite in the reaction. In the greywacke-paragneisses containing almandine no muscovite or sillimanite is found. The lack of muscovite may be explained by its total depletion in the formation of almandine. It is present in all other samples except those which possess a hornblende phase. The lack of sillimanite can be explained in another way. Its presence would be expected as both muscovite and quartz are present as reactants, however, the important minerals to consider are the products of the reactions. The formation of almandine garnet is favoured over sillimanite, hence, reaction (4) occurs instead of reaction (1). The intimate association of the almandine garnet-bearing paragneisses with the iron formation may have some influence on the reaction preferred.

iii) Pressure and Temperature of Metamorphism:

The pressure and temperature regime of the latest thermal event affecting the portion of the PAG studied is probably best illustrated by the metamorphic mineral assemblages found in the paragneisses. The key mineral assemblage of concern is the coexistence of orthoclase and sillimanite in the presence of quartz and muscovite. It might be argued that the mineral assemblage quartz, biotite, K-feldspar and almandine may also have some application to this end, but it represents an earlier thermal event and is stable over a far greater range than the dehydration of muscovite reaction. Hence, the geothermometer and geomanometer to be implemented will be the univariant equilibrium curve for reaction (1).

The univariant curve used for this reaction is after Althaus et al. (1970) (curve A, Fig. 22), and is plotted on the phase diagram of the Al_2SiO_5 stability field after Holdaway (1971) (triple point H, Fig. 22). This curve has the values 640° ± 10°C at 2.0 Kbars P_{H_2O}, and 670° ± 10°C at 3.5 Kbars P_{H_2O}. Through these points also pass the univariant curves for the polymorphic transition of andalusite/sillimanite, and the melting curve of granite (Luth et al., 1964, curve L, Fig. 22). A possible lower thermal limit of metamorphism is obviously 640° ± 10°C. This may be slightly lower, but certainly within the tolerances indicated as Holdaway's experiment involved the growth of sillimanite on fibrolitic seeds, hence fibrolite may exist somewhat below, (i.e. to the right), of the andalusite/ sillimanite univariant equilibrium curve presented. The upper thermal limit is the melting curve of granite, or 670° ± 10°C. Field evidence indicates that the PAG may be, at least in part, the protolith of local granodioritic orthogneisses. Campbell (1974) reports that paragneissic remnants enclosed by magnetiferous granodioritic gneiss and gradational contacts between the PAG rocks occur, suggesting such a relationship. Since melting of the PAG rocks occurs, the upper limit of metamorphism may be slightly higher than that stated above, but not significantly so, as recognizable PAG remnants within the orthogneisses are preserved.

A handle on the lithostatic pressures accompanying the above thermal limits can be gained from several sources. The absence of kyanite and presence of sillimanite-fibrolite suggests that pressures are not high. The absence of garnet coexisting with the three-phase assemblage

Fig. 22.

AL2SIO5 STABILITY FIELD

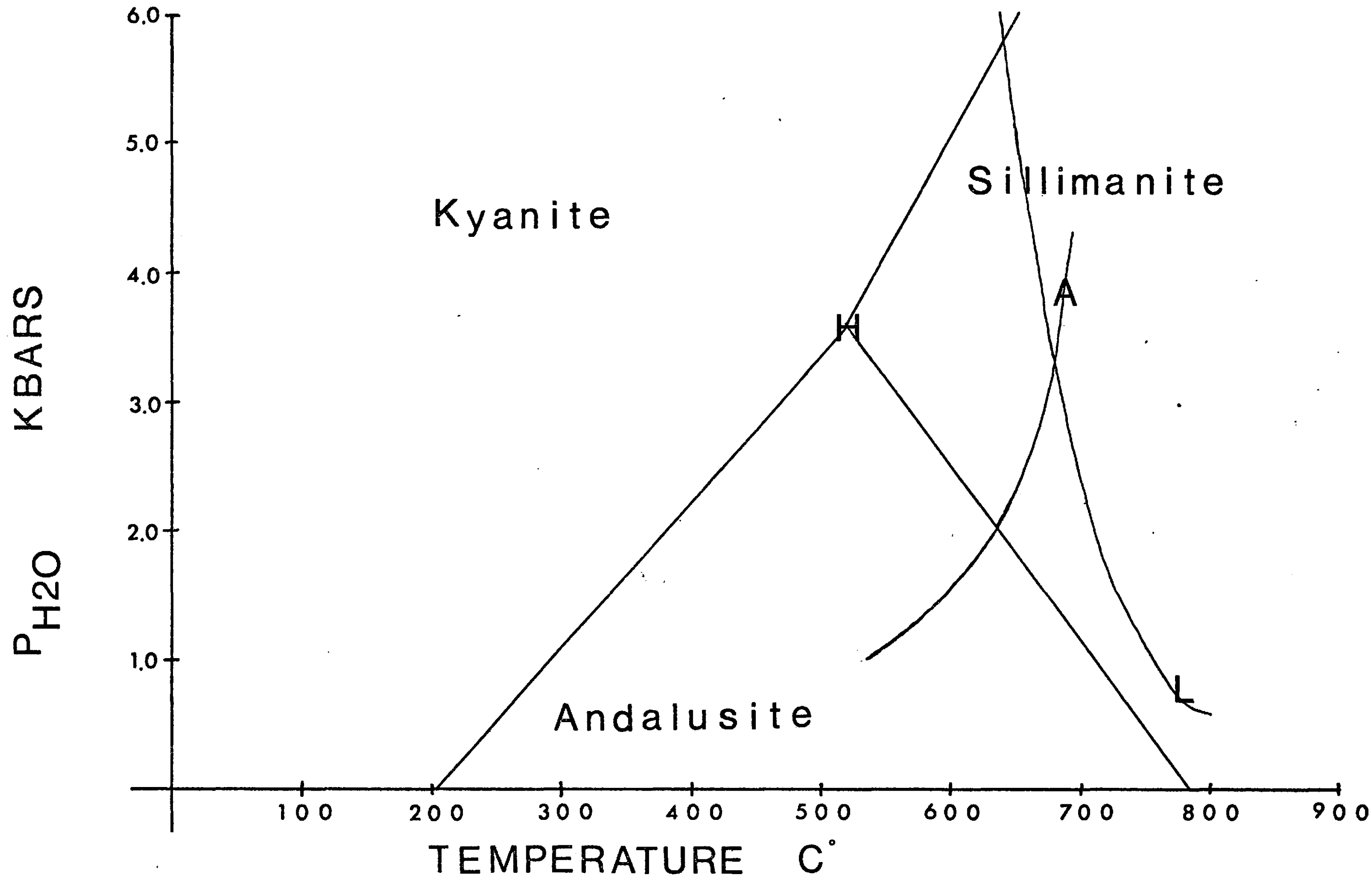

sillimanite-biotite-quartz substantiates a moderate to low pressure regime (Evans and Guidotti, 1966). Quantitatively, pressure values range between 2.0 Kbars P_{H_2O} and 3.5 Kbars P_{H_2O}, as shown in Fig. 22.

Thus, it is apparent that the last thermal event involved high temperatures and moderate to low pressures. Previous thermal events are severely masked by post-thermal deformation and later thermal events. However, the presence of biotitic metamorphic differentiation and the formation of almandine garnet porphyroblasts suggest temperatures of previous metamorphisms were lower than that of the last thermal event, but lithostatic pressures may have been higher. As a lower limit it is doubtful that any metamorphic event preserved in the PAG was of a lower grade than the Quartz-albite-epidote-almandine Subfacies of the Greenschist facies of metamorphism as described by Winkler (1967).

iv) Chemical Considerations With Respect to Metamorphism:

Mobile components will be the chemical considerations discussed. Mobile components which bear consideration are H_2O and O_2. CO_2, B, and F may be minor constituents. The dehydration of muscovite, equation (1) above, yields water. At the pressure-temperature regime existing in the latest metamorphism of the PAG water would be a mobile, supercritical fluid. In such a state water would tend to seek sites whose μ_{H_2O} was the lowest in the vicinity. The presence of migmatitic veins and small pegmatite sills in some of the outcrops of the greywacke-paragneiss sequence of the PAG may represent relict sites of low μ_{H_2O}. The large grain sizes of the pegmatites can be explained by hydrous anatexis of the surrounding rocks. Water would act as the fluid medium constantly supplying chemical constituents for large grain crystal growth.

Another mobile component, O_2, may also have been present during metamorphism. Little can be said concerning oxygen fugacities in the suite studied except that the lack of spessartine garnet, yet presence of almandine garnet suggests fO_2 was generally low.

The components CO_2, B and F should be considered. Their presence and effect on the bulk of the suite should be treated as being negligible as their very existence is only suggested in one sample, J73-088. Here calcite and siderite are found, hence CO_2 was a mobile component. Their net effect would be to lower the pressure and temperature of metamorphism of that particular facies of the meta-ultrabasic rocks.

v) Structural Considerations With Respect to Metamorphism:

Structural deformation has had several influences on the metamorphism of the PAG. The most pronounced effect is the formation of metamorphic differentiation. This is best displayed by the compositional layering of alternating quartzo-feldspathic and biotitic layers. This differentiation is parallel to the S_1 and S_2 foliations, hence defining these metamorphic planar fabrics. Another deformation associated phenomenon is the creation of pressure shadows. These were mentioned above and contain sutured quartz and K-feldspar grains adjacent to the almandine poikiloblasts but enclosed by the wrapping biotite foliation. These shadows escape the deformation event which wraps the biotite foliation about the perturbation and are essentially a window into the earlier history of the rock. Such histories may be masked by deformational events occurring after the formation of the shadow. In the PAG, D_3 would be a potential masking event, but evidence indicates this caused warping of axial traces, thus its masking of histories preserved in the pressure shadows would be minimal.

The growth of sillimanite-fibrolite is also closely connected to deformation in the PAG. This is brought out vividly in the wisps of fibrolite mats mentioned earlier. These indicate that fibrolite grew under an anisotropic stress field. However, the event that fibrolite formed from all muscovite grains in fold noses was also observed. This suggests that the thermal event associated with fibrolite growth was locally small enough that straining previous to this event became an important parameter in deciding the equilibrium position of reaction (1).

vi) Tectono-Thermo-Time Relations:

One of the ultimate aims of any metamorphic study is to attempt to unravel the geologic history hidden behind the metamorphic veil. This is achieved through careful mineralogical and textural studies supplemented by outcrop relations. From the preceding study of the PAG, the following outline of the metamorphic history can be deduced. Upper case alphanumerics represent discrete events but those labelled with lower case

Roman numerals are geologically contemporaneous events.

A) formation of original bedding S_0

B) formation of biotite-muscovite-hornblende, S_1 foliation

C) thermal assimilation of almandine garnet

D) garnet rotation plus suturing and straining of adjacent sialic minerals

E) i) folding, creating "en echelon" F_2 isoclinal and kink folds and straining of muscovite grains

ii) formation of S_2 biotite hornblende foliation some of which crenulate S_1

iii) formation of muscovite and quartz porphyroblasts in the quartzite sequence

F) F_3 folding and warping of F_2 axial trace

G) anisotropic growth of fibrolite

H) isotropic growth of fibrolite

This data is presented graphically in Fig. 23 which separates thermal and tectonic events but correlates each through the common parameter, time.

Fig. 23.

TECTONO-THERMO-TIME PLOT

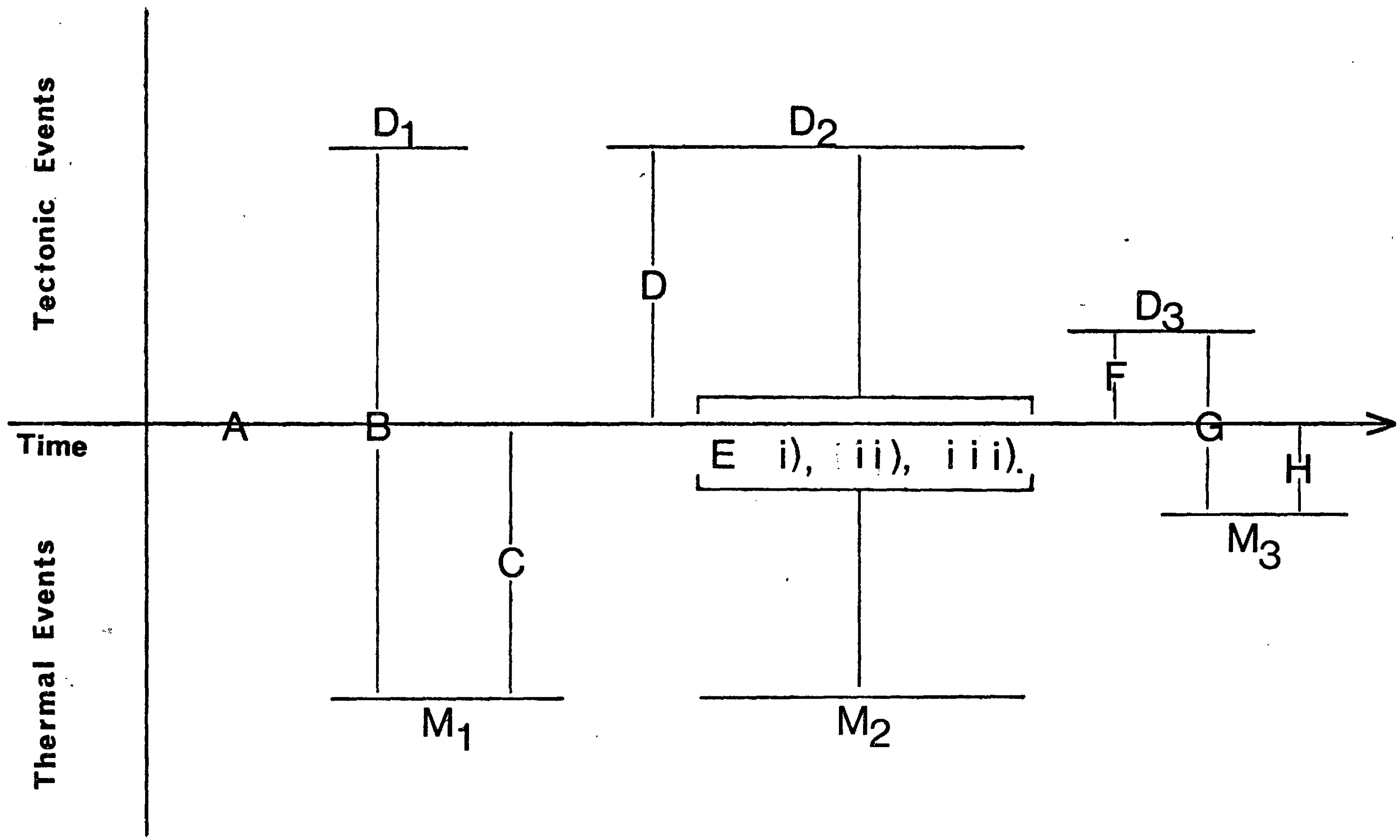

vii) Contributions Towards an Orogenic Model:

The above metamorphic study has brought to the forefront a number of interesting facets concerning the PAG. First, it has been shown that the latest metamorphic events involved low to moderate pressures at high temperatures. Secondly, pre-M_3 metamorphic events may have occurred at somewhat lower temperatures and higher pressures. Thirdly, no mineralogical or textural evidence suggests that thermal and/or tectonic events of the Kenoran orogeny affected the PAG.

Hence, the accompanying tectono-thermo-time plot (Fig. 23) is a metamorphic record of the Hudsonian orogeny in the PAG-Ellice Hills sheet. This record indicates that near the beginning of the orogen thermal and tectonic events were quite severe and metamorphism was prominent. As time progressed thermal and tectonic events did not remain completely in step and both distinct thermal and tectonic imprints were cast into the PAG. Finally by the time D_3 was reached tectonic events lost their severity and M_3, even though a high temperature event, was accompanied by low to moderate pressures.

One explanation for this progression of events is that this section of the PAG was a slowly rising block. Initial pressures would be moderate to high with moderate temperatures. As the block rose tectonic events would arise from the simple physical interaction with surrounding blocks or rock masses. This tectonism would become substantially less as the rising block approached a static state. Lithostatic pressures would also decrease as the block approached physical equilibrium. The increase in thermal input accompanied by low to moderate pressure can be explained by the injection of high level intrusions and large sills. Both granodioritic sills and other large bodies are present in outcrop, (mentioned earlier).

The size of these blocks would be large enough so that much of the study area would be encompassed within one block. If such blocks existed, then the presence of kyanite in a block to the west of the study area might be explained by differential uplift. Schau (1974) reports this occurrence of kyanite and mentions that it may be explained by either differential uplift or by thermal increase to the east. In light of the pressure-temperature regime determined for the PAG in the study area it is obvious a temperature increase accompanied by a pressure drop is needed. Otherwise it is impossible to move from the kyanite field to the univariant curve for the dehydration reaction of muscovite without passing through the stability field of andalusite.

REFERENCES

Althaus, E., Karothe, E., Nitsch, K.H., and Winkler, H.G.F. (1970). An Experimental Re-examination of the Upper Stability Limit of Muscovite and Quartz. Neues Jahrb. Mineralogie Monatsh., Vol. 7, pp. 289-336.

Brown, G.C., Hughes, D.J., and Esson, J. (1973). New X.R.F. Data Retrieval Techniques and Their Application to U.S.G.S. Standard Rocks. Chemical Geology, Vol. 11, pp. 223-229.

Cameron, W.E., and Ashworth, J.R. (1972). Fibrolite and Its Relationship to Sillimanite. Nature, Physical Sciences, Vol. 235, No. 59.

Campbell, F.H.A. (1973). Sedimentary Rocks of the Prince Albert Group, District of Keewatin. G.S.C. Paper 73-1, Part A, 141 p.

Campbell, F.H.A. (1974). Paragenesis of the Prince Albert Group. G.S.C. Paper 74-1, Part A, 159 p.

Davidson, A. (1970). Pre-Cambrian Geology, Kaminak Lake Map Area, District of Keewatin. G.S.C. Paper 69-51.

Davidson, A. (1972). The Rest of the Churchill Province, in Variations in Tectonic Styles in Canada. G.S.C. Special Paper No. 11, pp. 402-433.

Deer, F.R.S., Howie, R.A., and Zussman, J. (1966). An Introduction to the Rock-Forming Minerals. Longman, London.

Evans, B.W., and Guidotti, C.V. (1966). The Sillimanite-Potash Feldspar Isograd in Western Maine, U.S.A. Contrib. Mineral. Petrol., Vol. 12, No. 1, pp. 25-62.

Frisch, T. (1973). Granitic and Associated Rocks of the Committee Bay Area, Districts of Keewatin and Franklin. G.S.C. Paper 73-1, Part A, 145 p.

Frisch, T. (1974). Geological Studies in the Prince Albert Hills, Western Melville Peninsula, District of Franklin. G.S.C. Paper 74-1, Part A, 163 p.

Guidotti, C.B. (1963). Metamorphism of Pelitic Schists. Amer. Mineral. 48, pp. 772-791.

Heywood, W.W. (1961). Geological Notes, Northern District of Keewatin. G.S.C. Paper 61-18.

Heywood, W.W. (1966). Geological Notes, Northern District of Keewatin and Southern Melville Peninsula, District of Franklin, N.W.T. G.S.C. Paper 66-40.

Heywood, W.W. (1974). Geological Reconnaissance of Northern Melville Peninsula, District of Franklin (Parts of 47A,B,C,D). G.S.C. Paper 74-1, Part A, 381 p.

Holdaway, M.J. (1971). Stability of Andalusite and the Aluminum Silicate Phase Diagram. Amer. J. Sci., Vol. 271, p. 97.

Hyndman, D.W. (1972). Petrology of Igneous and Metamorphic Rocks. McGraw-Hill, New York.

Kerr, P.G. (1959). Optical Mineralogy, 3rd Edition. McGraw-Hill, New York.

Luth, W.C., Johns, R.H., and Tuttle, O.F. (1964). The Granite System at Pressures of 4 to 10 Kbars. J. Geophys. Res., Vol. 69, pp. 759-773.

Marchand, M. (1973). Determination of Rb, Sr and Rb/Sr by X.R.F. Tech. Memo 73-2, Dept. of Geology, McMaster University, Hamilton, Ontario, Canada.

McCracken, D.D. (1965). A Guide to Fortran IV Programming. J. Wiley and Sons, New York.

Moorhouse, W.W. (1959). The Study of Rocks in Thin Section. Harper and Row, New York.

Schau, M. (1973). Volcanic Rocks of the Prince Albert Group. G.S.C. Paper 73-1, Part A, 175 p.

Schau, M. (1974). Volcanic Rocks of the Prince Albert Group, District of Keewatin. G.S.C. Paper 74-1, Part A, 187 p.

Spry, A. (1969). Metamorphic Textures. Pergamon Press Ltd., London.

Stockwell, C.H. (1972). Revised Pre-Cambrian Time Scale for the Canadian Shield. G.S.C. Paper 72-52.

Turner, F.J. (1968). Metamorphic Petrology, Mineralogical and Field Aspects. McGraw-Hill, New York.

Turner, F.J., and Weiss, L.E. (1963). Structural Analysis of Metamorphic Tectonics. McGraw-Hill, New York.

Williams, H., Turner, F.J., and Gilbert, C.M. (1954). Petrography, An Introduction to the Study of Rocks in Thin Section. W.H. Freeman and Co., San Francisco.

Winkler, H.C.F. (1967). Petrogenesis of Metamorphic Rocks, Revised 2nd Edition. Springer-Verlag, New York.

Wright, C.M. (1967). Geology of the Southern Barren Grounds, Parts of the Districts of MacKenzie and Keewatin. G.S.C. Memoir 350.

APPENDIX A

PETROGRAPHIC DESCRIPTIONS

AND

SKETCHES

Sample: J73-032 UTM Coordinates: 434100 Easting
7482000 Northing

Classification: Quartz-Feldspar-Biotite-Muscovite Paragneiss with Sillimanite Knots

Modal Abundances: Quartz -- 34%
Feldspar-K-spar -- 14% (Orthoclase)
-Plagioclase -- 3% (Andesine An 45)
Biotite -- 20%
Muscovite -- 15%
Sillimanite -- 12%
Tourmaline -- 1% (Schorlite)
Zircon -- 1%
Mafic Oxide -- less than 1%
Sericite -- less than 1%

Textures:

The thin section contains discontinuous layers of biotite plus muscovite in a matrix of quartzo-feldspathic material with porphyroblasts of sillimanite (fibrolite), and muscovite. The biotite occurs as discrete to matted blades which tend to be subhedral to anhedral. The biotite layers are not continuous but display a preferred orientation and appear to be warped around sillimanite porphyroblasts. Some biotite grains are interlayered with muscovite grains and inclusions of quartz and more often zircon are observed. Occasional biotite and muscovite blades are found inclined to the preferred orientation. The muscovite grains are also subhedral to anhedral and display a prevalent corrosion by quartz (see below). Grain sizes of both the biotite and muscovite grains range from 0.1 mm to 1.8 mm. The micaceous layers are weakly to moderately foliated.

The quartzo-feldspathic matrix is mainly composed of quartz, some orthoclase, and little plagioclase. This matrix tends to be granoblastic and shows two distinctive grain sizes. One ranging from 0.4 mm to 1.8 mm, and the other less than 0.4 mm. The larger grain sizes tend to be limited to quartz and K-spar only. These grains are anhedral with distinct grain boundaries and undulose extinction. There is no preferred orientation although some grains are elongated parallel to the biotite grains mentioned above. The smaller size material includes quartz, K-spar and plagioclase. These grains are always anhedral and usually equidimensional. The plagioclase grains are few and may contain some sericitization, hence the Michel-Levy determination of sodium/calcium content may be less accurate than desired. Within this sialic matrix occur scattered, isolated, subhedral to anhedral grains of schorlite.

The sillimanite-fibrolite-muscovite porphyroblasts are anhedral being composed of matted fibrolite and poikilitic, subhedral to anhedral muscovite grains. The fibrolite is found in several forms ranging from tightly packed, randomly oriented, fibers to radiating mats and swirled wisps (see sketch). Inclusions and embayments in the muscovite include quartz, K-spar and fibrolite with reaction rims around the quartz and K-spar. The grain size range of the porphyroblasts is 2.5 mm to 3.5 mm.

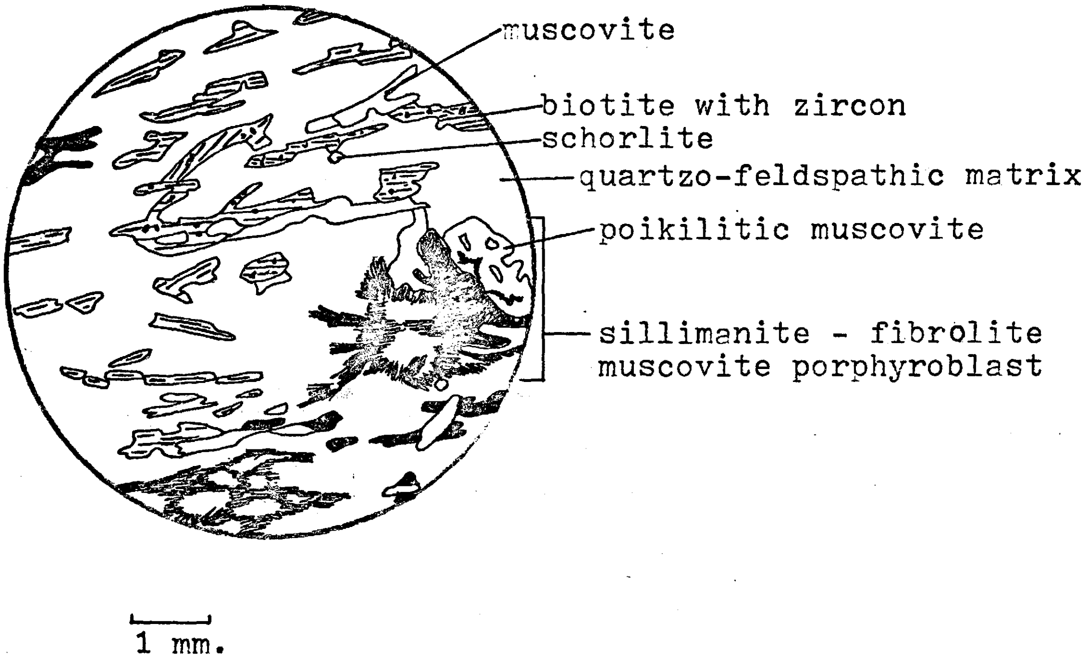

PLANE POLARIZED LIGHT

SAMPLE J73-032

Sample: J73-036 UTM Coordinates: 431050 Easting

7478750 Northing

Classification: Quartz-Feldspar-Biotite Paragneiss

Modal Abundances: Quartz -- 37%

Feldspar-K-spar -- 26% (Orthoclase and Microcline)

-Plagioclase -- 9% (Labradorite An 54 - An 55)

Biotite -- 24%

Muscovite -- 1%

Zircon -- 1%

Mafic Oxide -- 1%

Sericite -- 1%

Textures:

The thin section is composed of a quartzo-feldspathic groundmass in which discontinuous, sub-parallel layers of biotite are found. The quartzo-feldspathic groundmass contains quartz, orthoclase, microcline and labradorite, all of which exhibit a granoblastic texture with clear grain boundaries. All grains are anhedral but the grain size is variable. The labradorite grains tend to be the largest ranging from 0.2 mm to 0.8 mm, while the quartz and K-spar grains range from 0.1 mm to 0.6 mm. The plagioclase grains are noted to be altered to sericite, but this sericitization is by no means severe. Small inclusions of quartz are often found in the feldspars. These inclusions are usually rounded to subrounded anhedra which possess distinct grain boundaries. Such inclusions seem to be limited to a maximum of approximately two per grain.

The discontinuous biotite layers are composed of subhedral to anhedral blades of biotite which occur both as discrete blades and as masses of parallel to sub-parallel blades. The biotites tend to exhibit a preferred orientation even though slight, but frequent, variations occur. Inclusions in the biotites include zircons and embayments of quartz which often have reaction rims with the biotite. Grain sizes of the biotites range from 0.2 mm to 1.8 mm. Biotite grains are occasionally cut by small muscovite grains. These muscovite grains range in size from 0.15 mm to 0.20 mm and are subhedral to anhedral in form. The biotite layers are weakly to moderately foliated.

PLANE POLARIZED LIGHT

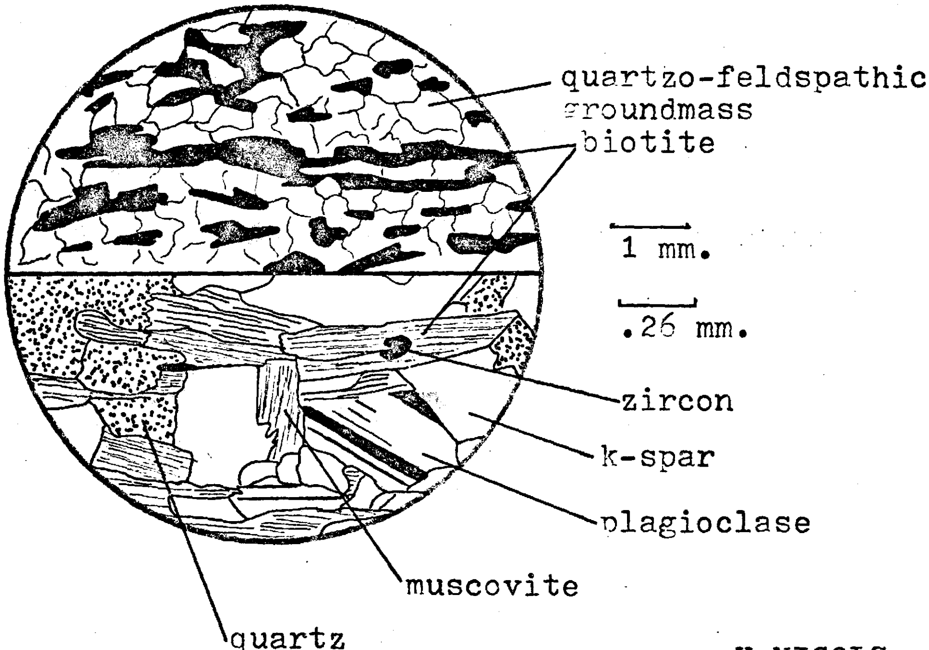

X-NICOLS

SAMPLE J73-036

Sample: J73-040 UTM Coordinates: 434440 Easting

7480600 Northing

Classification: Quartz-Feldspar-Biotite Paragneiss

Modal Abundances: Quartz -- 37%

Feldspar-K-spar -- 9% (Orthoclase and Microcline with inclusions)

-- 18% (Orthoclase without inclusions)

-Plagioclase -- 9%

Biotite -- 15%

Sericite -- 7%

Muscovite -- 3%

Zircon -- 1%

Corundum -- 1%

Mafic Oxide -- 1%

Textures:

The thin section is composed of isolated biotite grains and porphyroblasts of corundum in a quartzo-feldspathic groundmass. The biotite grains are subhedral to anhedral blades with an ill-defined preferred orientation, although one was noted in the outcrop. The biotite grains display distinct green lamellae parallel to their long axis and subhedral to anhedral muscovite blades are associated. The muscovite is also associated closely with sericitized feldspar suggesting it may be the result of complete sericitization. Some biotite grains display boundaries which are not sharp but blend into surrounding K-spar or quartz. No alteration or exsolution phenomena are seen at such boundaries. The grain size of the biotites range from 0.1 mm to 0.7 mm, and muscovite from 0.1 mm to 0.4 mm. The biotites possess inclusions of zircon and are poorly foliated.

The quartzo-feldspathic groundmass comprises 70 to 75% of the section and is generally granoblastic. The main components are large anhedra,(0.9 mm to 2.5 mm) of quartz and K-spar. Grain boundaries are sharp, but irregular and extinction may be sharp or undulose. No alteration of these two components is observed. Within the above grains inclusions of both K-spar (orthoclase), and plagioclase are found. These inclusions occur both within the grain proper and at grain boundaries and may be euhedral, subhedral or anhedral in form, but always possess distinct grain boundaries. Alteration of the feldspar inclusions to sericite, and even muscovite, is omnipresent occurring along cleavage planes and twinning planes. Anhedral quartz inclusions are also found and may occur either in larger quartz or K-feldspar grains. The grain size of these inclusions ranges from 0.08 mm to 0.6 mm. Not all grains possess inclusions but few microcline grains lack any.

The small porphyroblasts of corundum range in size from 0.1 mm to 0.3 mm and in form from euhedra to anhedra. Such porphyroblasts may possess inclusions of anhedral quartz (approximately 0.05 mm).

PLANE POLARIZED
LIGHT

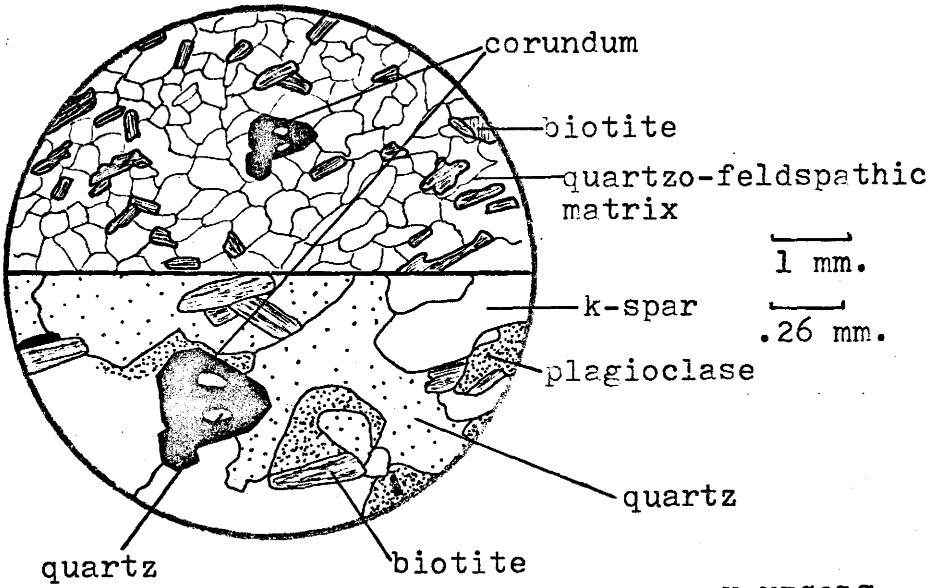

X-NICOLS

SAMPLE J73-040

Sample: J73-051 UTM Coordinates: 423530 Easting
7474080 Northing

Classification: Quartz-Feldspar-Biotite-Garnet Paragneiss

Modal Abundances: Quartz -- 35%
Feldspar-K-spar -- 18% (Orthoclase)
-Plagioclase -- 19% (Labradorite An 50)
Biotite -- 23%
Almandine Garnet -- 3%
Zircon -- less than 1%
Mafic Oxide -- less than 1%

Textures:

The thin section is comprised of continuous to discontinuous layers of deformed biotite which sit in a quartzo-feldspathic groundmass which also contains porphyroblasts of almandine. The biotite layers are composed of subhedral to anhedral blades of biotite which show no preferred orientation but are crenulated displaying essentially two preferred orientations approximately orthogonal to one another (see sketch). (It should be noted that this thin section was cut orthogonal to the plane defined by the principal foliation to exemplify the crenulations.). The biotite grains often contain inclusions of both quartz and zircons with alteration of some of the biotite grains to mafic oxide. Embayment of the biotites can occur by either quartz, K-spar or plagioclase. Grain size of the biotites ranges from 0.25 mm to 1.5 mm. Texturally the biotites are moderately to well foliated.

The quartzo-feldspathic groundmass is composed of quartz, orthoclase and labradorite. The texture of this groundmass can be expressed as granoblastic but some rather small grains do occur. All three phases occur as anhedra and definite grain boundaries are usually found. Grain sizes vary from 0.1 mm to 1.8 mm, but most are between 0.3 mm and 1.0 mm. No sericitization of the feldspars occurs and very few inclusions are formed in the quartzo-feldspathic grains.

The almandine garnet porphyroblasts are anhedral and vary in size from 0.3 to 0.5 mm. These porphyroblasts are often fractured and may possess inclusions of either mafic oxide, K-spar, or quartz. The almandine grains are usually bounded at least on one side (and several times on all three) by biotite grains. The grain boundaries of the garnets are sharp and no helitic textures are preserved. The almandines are usually associated at, or close to, a junction of biotites whose orientations are juxtaposed. However, not all crenulations are associated with almandine porphyroblasts.

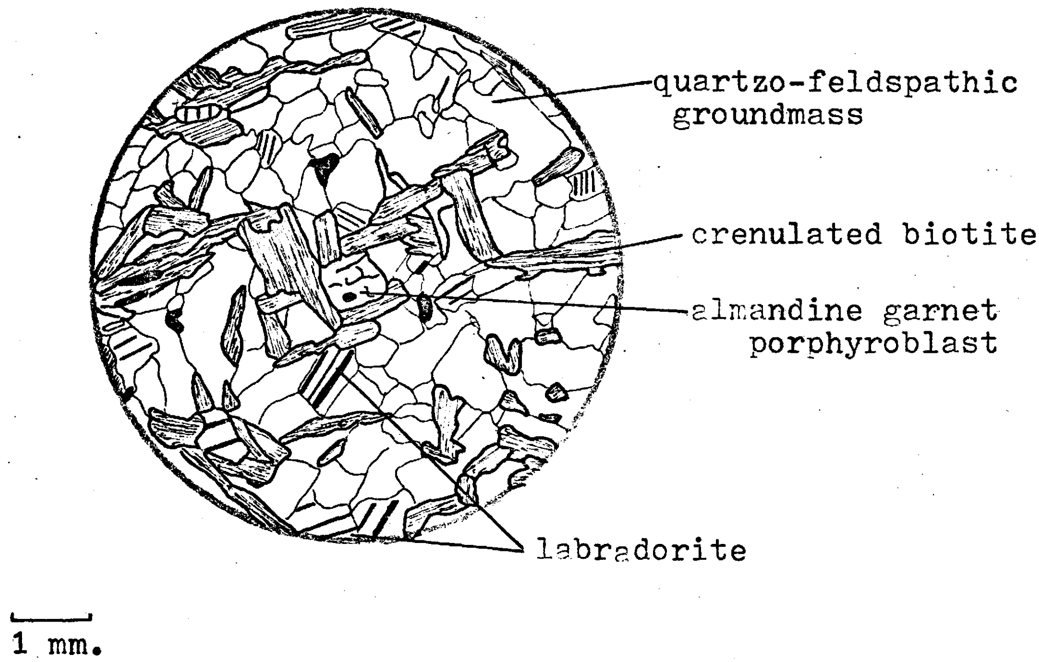

X-NICOLS

SAMPLE J73-051

Sample: J73-050-2 UTM Coordinates: 423300 Easting
7474500 Northing

Classification: Quartz-Feldspar-Biotite-Almandine Paragneiss

Modal Abundances: Quartz -- 34%

Feldspar-K-spar -- 19% (Orthoclase)

-Plagioclase -- 14% (Labradorite An 68)

Biotite -- 24%

Almandine Garnet -- 7%

Zircon -- 1%

Mafic Oxide -- 1%

Textures:

The thin section is composed of continuous layers of biotite which are deformed by almandine garnet porphyroblasts. Alternating with the micaceous layers are bands of quartzo-feldspathic material. The biotite layers are comprised of subhedral to anhedral blades of biotite which tend to have a preferred orientation although these layers can be deformed around almandine porphyroblasts. The biotites are sometimes cut by other inclined biotites and may possess inclusions of quartz and K-spar, along with zircons. Alteration of some biotite to a black-brown mafic material sometimes occurs. The biotite grains have well defined grain boundaries and range in size from 0.1 mm to 2.1 mm, with a large majority being larger than 0.6 mm, and are texturally well foliated.

The quartzo-feldspathic layers have three phases present: quartz, orthoclase and labradorite. The quartz and K-spar grains are anhedral and possess a range of grain sizes from 0.1 mm to 1.8 mm. The larger grains show undulose extinction, but grain boundaries for all sizes are distinct. Anhedral inclusions of quartz and slight sericitization of some K-spar grains periodically occurs. The plagioclase grains are subhedral to anhedral in form and display only minor sericitization along twin planes. Grain boundaries of the plagioclase are distinct and grain sizes range from 0.4 mm to 1.8 mm.

The almandine garnet porphyroblasts occur as anhedra ranging in size from 3.5 mm to 5.4 mm. These grains show fracturing and inclusions of black mafic material plus quartz, K-spar, and biotite. The quartz and K-spar grains occur as parallel to sub-parallel trains within the garnet displaying a preferred orientation. This orientation is inclined to the preferred orientation exhibited by the biotite foliation in the rock itself. This juxtaposition of orientations may indicate that the garnet has been rotated, thus displaying a helitic texture. The external biotites are wrapped around the garnet creating and "eye" effect. In the shadows adjacent to the nucleus of the "eye" one finds large anhedral grains of both quartz and K-spar. The quartz displays both sutured and gently undulating boundaries plus undulose extinction. The sialic material becomes more like the quartzo-feldspathic layers as one moves away from the garnet porphyroblasts and into these layers. The garnet porphyroblasts are not always isolated from each other but may occur in groups as high as three.

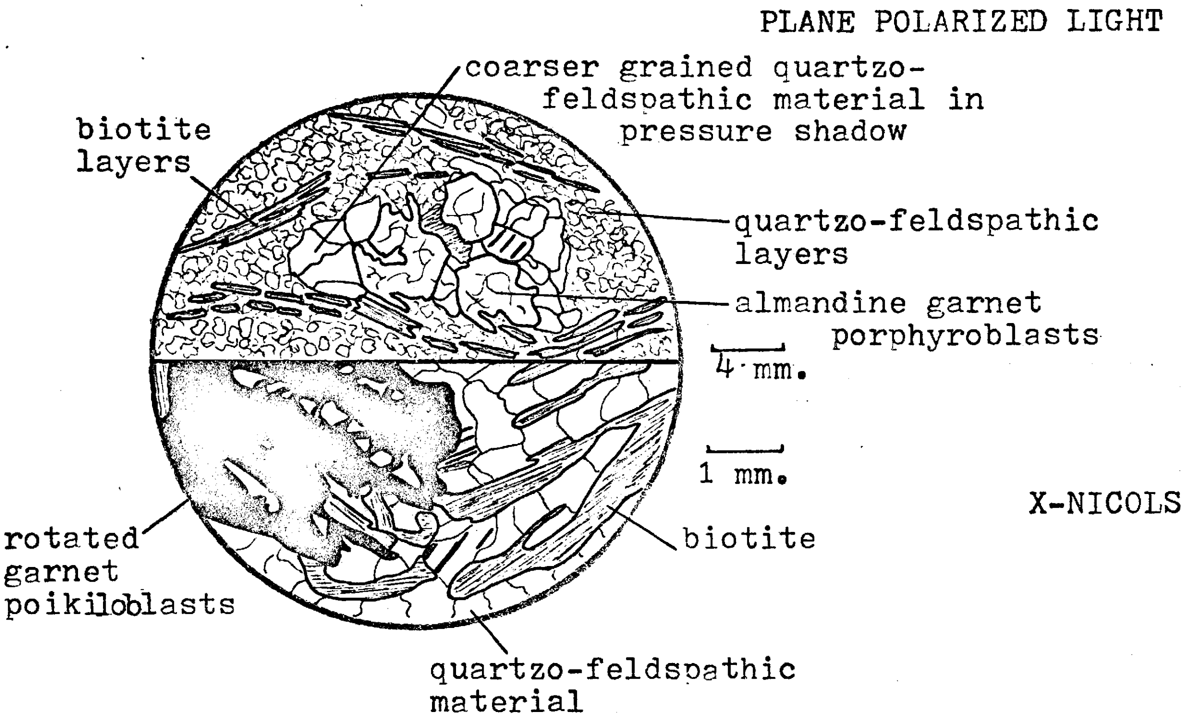

SAMPLE J73-050-2

Sample: J73-048 UTM Coordinates: 432910 Easting

7481680 Northing

Classification: Kink Folded Quartz-Feldspar-Biotite Paragneiss

Modal Abundances: Quartz -- 31%

Feldspar-K-spar -- 17% (Orthoclase)

-Plagioclase -- 8% (Labradorite An 59)

Biotite -- 29%

Muscovite -- 6%

Sillimanite -- 4% (Fibrolite)

Sericite -- 2%

Tourmaline -- 1% (Schorlite)

Zircon -- 1%

Mafic Oxide -- 1%

Textures:

The thin section contains continuous layers of biotite and muscovite with alternating layers of quartzo-feldspathic grains. The micaceous layers are predominantly composed of subhedral to anhedral blades of biotite, however, anhedral muscovite also occurs. The biotite grains exhibit three preferred orientations. Two of these orientations are represented by the fold limbs of the tight micro-isoclinal (almost kinked) folds and the third is parallel to the axial planes of the folds and is found where the limbs are tightly packed, forming a foliation (see sketch). The biotite grains are sometimes interstratified with both quartz and K-spar grains which tend to have long axes parallel to the biotite grains, at that particular location. Some biotite grains also possess zircon inclusions. Biotite grains range in size from 0.3 mm to 1.2 mm, and show some alteration to both brown and black mafic oxides. (It should be noted that due to the continuity of the biotite layers the grains often appear longer than they actually are.). Also occurring in the micaceous layers are muscovite grains mentioned above. These may occur anywhere within the layers and may be parallel to the biotite blades or crosscut the foliation. When muscovite grains occur in the fold nose they may be corroded by quartz, and the association of both K-spar and sillimanite-fibrolite is usually intimate. Texturally these micaceous layers are well foliated and crenulated.

The quartzo-feldspathic material consists of granoblastic phases of quartz, orthoclase, and labradorite. All grains are anhedral with sharp grain boundaries. The quartz and K-spar grains sometimes have inclusions of each other or the same material but with distinct boundaries about the inclusions. The plagioclase grains are slightly altered to sericite. The grain sizes of these above phases range from 0.5 mm to 0.9 mm.

Within the quartzo-feldspathic material isolated anhedra of schorlite occur. Grain sizes of the schorlite range from 0.1 mm to 0.4 mm. Grains are generally fractured and may include embayments of quartz.

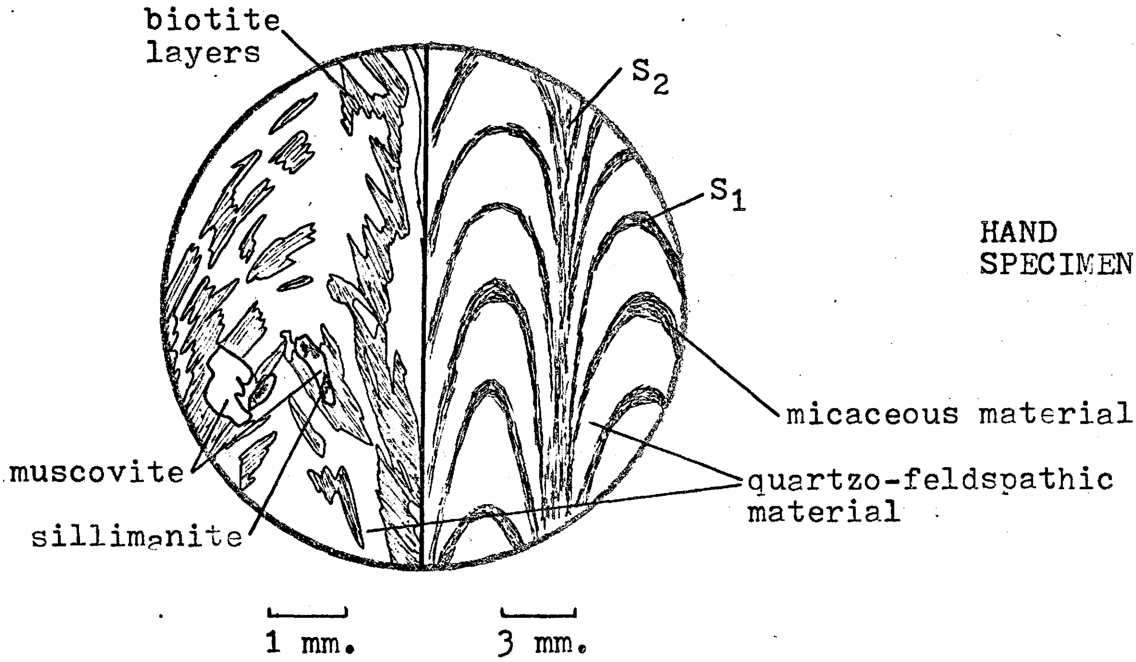

PLANE POLARIZED LIGHT

SAMPLE J73-048

Sample: J73-004 UTM Coordinates: 377400 Easting

7458800 Northing

Classification: Kink Folded Quartz-Feldspar-Biotite-Hornblende Paragneiss

:

Modal Abundances: Quartz -- 22%

Feldspar-K-spar -- 9% (Orthoclase)

-Plagioclase -- 3% (Andesine An 45)

Biotite -- 34%

Hornblende -- 29%

Zircon -- 3%

Mafic Oxide -- less than 1%

Textures:

The rock contains alternate layers of quartzo-feldspathic material and biotite-hornblende which are tightly folded into "en echelon" kink folds (average inter-limb angle approximately 30 degrees). The quartzo-feldspathic layers are thinner than the biotite-hornblende layers and the grains show no preferred orientation. Both the quartz and K-spar grains found in these layers are granoblastic, anhedral, displaying sharp, irregular grain boundaries. Grain sizes in this layer range from 0.2 mm to 2.5 mm. Anhedra of plagioclase are found in this layer also, along with both biotite and hornblende grains.

The biotite-hornblende layers are the most prominent defining the foliation-gneissosity and the kink folds. The biotite is found as subhedral to anhedral blades parallel to the foliation. However, some biotite grains (and less often hornblende) are inclined to this foliation,(average angle of inclination 36 degrees), cross-cutting other biotite and hornblende grains. Some biotites show a poikilitic texture with minor inclusions of quartz grains and zircons. Hornblende grains are subhedral to anhedral displaying both longitudinal and cross sections. Some hornblende grains show inclusions of quartz and zircons. Grain sizes of both biotite and hornblende are variable ranging from 0.15 mm to 3.0 mm.

The limbs of the folds tend to be continuous but occasionally exhibit biotite blades bent around cross-sectional hornblende grains (see sketch). The fold noses are best defined by biotite blades which are not bent at the vertex but tend to be the juxtaposition of two different orientations forming sharp kink noses. Both hornblende and quartzo-feldspathic material are found in the fold noses but interior to the biotites. The hornblende-biotite layers are well foliated.

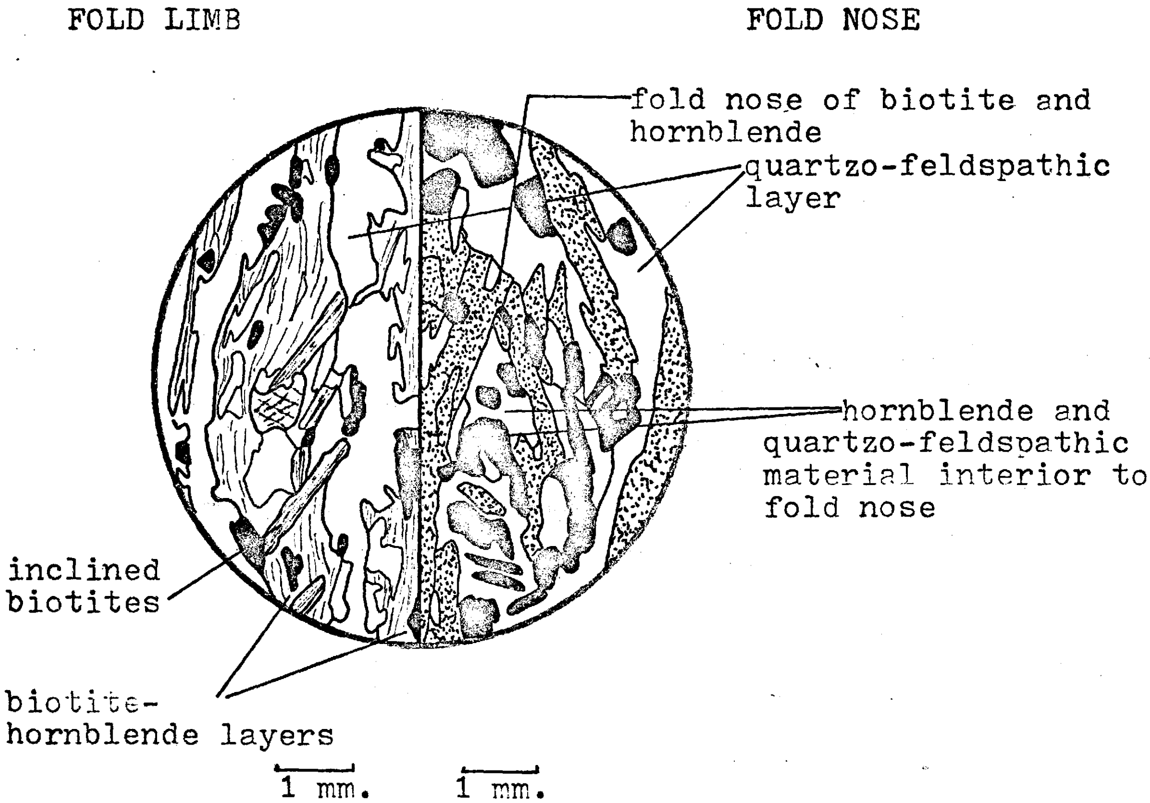

PLANE POLARIZED LIGHT

SAMPLE J73-004

Sample: J73-015 UTM Coordinates: 384410 Easting

7459160 Northing

Classification: Garnetiferous Amphibolite Gneiss

Modal Abundances: Quartz -- 16%

Feldspar-K-spar -- 3% (Orthoclase)

-Plagioclase -- 2% (Labradorite An 59)

Biotite -- 5%

Hornblende -- 62%

Almandine Garnet -- 8%

Sericite -- 1%

Zircon -- 1%

Mafic Oxide -- 2%

Textures:

The thin section is composed mainly of alternating layers of amphibole and quartzo-feldspathic material with garnet poikiloblasts. The chief phase present in the amphibole layers is hornblende, but small anhedra of quartz and less often plagioclase and biotite can be found. No obvious preferred orientation exists but some grains tend to have long axes which are sub-parallel to those of other amphibole grains. The amphiboles are warped around garnet poikiloblasts, although some amphibole grains are found within the poikiloblasts. Little alteration of the hornblende grains is seen however, inclusions of zircon and brown mafic oxide do occur. The plagioclase is somewhat altered to sericite and biotite grains are either altered to a brown mafic oxide or severely invaded by quartz along cleavage planes. This invading leads to "pinch and swell" type structures in the biotite grains. Grain sizes of the biotites in these layers range from 0.1 mm to 0.4 mm. The hornblende grains possess distinct grain boundaries and grain sizes range from 0.15 mm to 2.0 mm. Texturally the hornblende layers range from decussate to weakly foliated.

The quartzo-feldspathic layers are composed of anhedra of quartz and labradorite with randomly oriented anhedral biotite blades. The quartz and plagioclase grains possess distinct grain boundaries but the biotite grains have highly irregular and hazy boundaries. The plagioclase grains show alteration to sericite. Grain sizes of the quartz and feldspars vary from 0.05 mm to 0.4 mm and the biotite grains in these layers from 0.05 mm to 0.4 mm. Occasionally some anhedral grains of hornblende are found in the quartzo-feldspathic layers. Texturally these layers may be expressed as sub-granoblastic.

The almandine garnet present occurs as poikiloblasts. The original garnet is highly fractured and most of the garnet grains forming a large poikiloblast range from 0.05 mm to 1.0 mm and are very anhedral. Inclusions within the poikiloblast are of three phases, quartz, K-spar, and hornblende. Alteration of the garnet to a brown mafic oxide is found along fractures. Poikiloblasts of garnet range from approximately 3.0 mm to 7.0 mm.

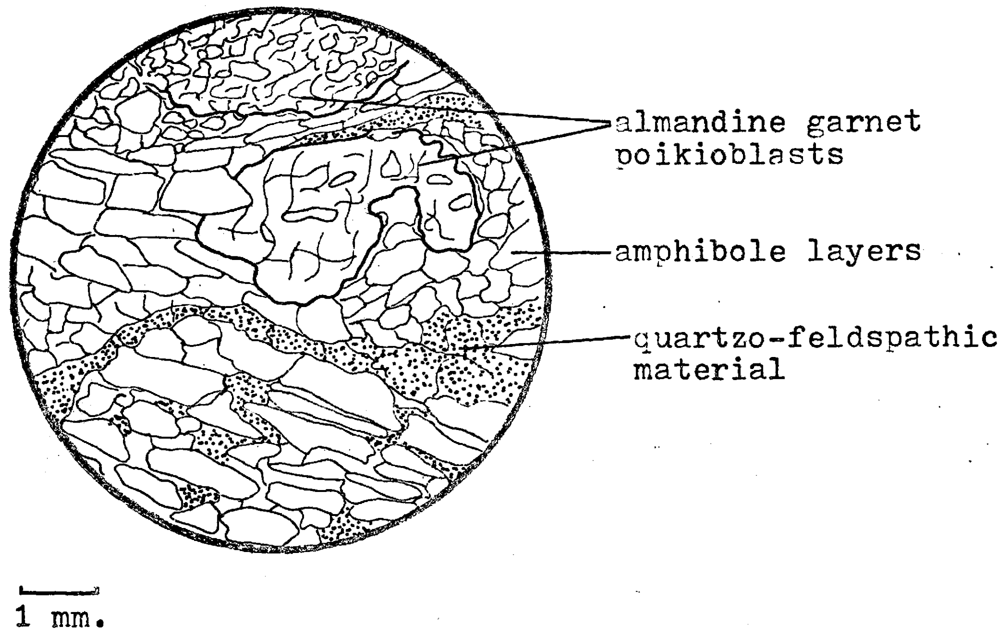

PLANE POLARIZED LIGHT

SAMPLE J73-015

Sample: J73-061 UTM Coordinates: 424990 Easting

7476090 Northing

Classification: Quartz-Feldspar-Biotite Paragneiss with Quartz-Muscovite-Sillimanite Porphyroblasts

Modal Abundances: Quartz -- 36%

Feldspar-K-spar -- 22% (Orthoclase)

-- 5% (Microcline)

-Plagioclase -- 5% (Labradorite An 60)

Biotite -- 4%

Muscovite -- 8%

Sillimanite -- 10% (Fibrolite)

Tourmaline -- 3% (Schorlite)

Sericite -- 3%

Corundum -- 1%

Mafic Oxide -- less than 1%

Textures:

The thin section shows that the rock is composed of a quartzo-feldspathic-biotitic groundmass with quartz and sillimanite-fibrolite-rich porphyroblasts. The groundmass is composed of five phases, quartz, orthoclase, microcline, labradorite and biotite. The quartz and orthoclase grains are anhedral while the microcline and plagioclase are subhedral to anhedral. Grain boundaries are sharp but small anhedral inclusions of any one or more of the phases may be present. Alteration of the feldspars along cleavage and twin planes to sericite also occurs. Both the quartz and orthoclase exhibit undulose extinction. The grain size of the above four phases ranges from 0.05 mm to 0.4 mm and the texture is best described as being granoblastic. The groundmass also contains subhedral to anhedral schorlite and biotite grains. The biotites show a poor preferred orientation although in hand specimen it is more obvious. Alteration of the biotites to a brown mafic oxide does occur. Grain sizes of the schorlite range from 0.1 mm to 0.2 mm and 0.1 mm to 1.0 mm for the biotite grains.

The quartz-sillimanite-fibrolite porphyroblasts are large ranging in size from 0.5 cm to 2.5 cm. The porphyroblasts possess a preferred orientation with their long axis being sub-parallel to parallel to the biotite foliation seen in hand specimen. The porphyroblasts contain a nucleus rich in subhedral to anhedral muscovite and anhedral sillimanite-fibrolite but a margin rich in anhedral quartz with minor orthoclase. The marginal grains have long axes essentially parallel to each other and the long axis of the porphyroblast itself. Grain sizes of the quartz vary from 0.2 mm to 1.8 mm. The muscovite grains are highly corroded by quartz from which sillimanite and possibly K-spar formed.

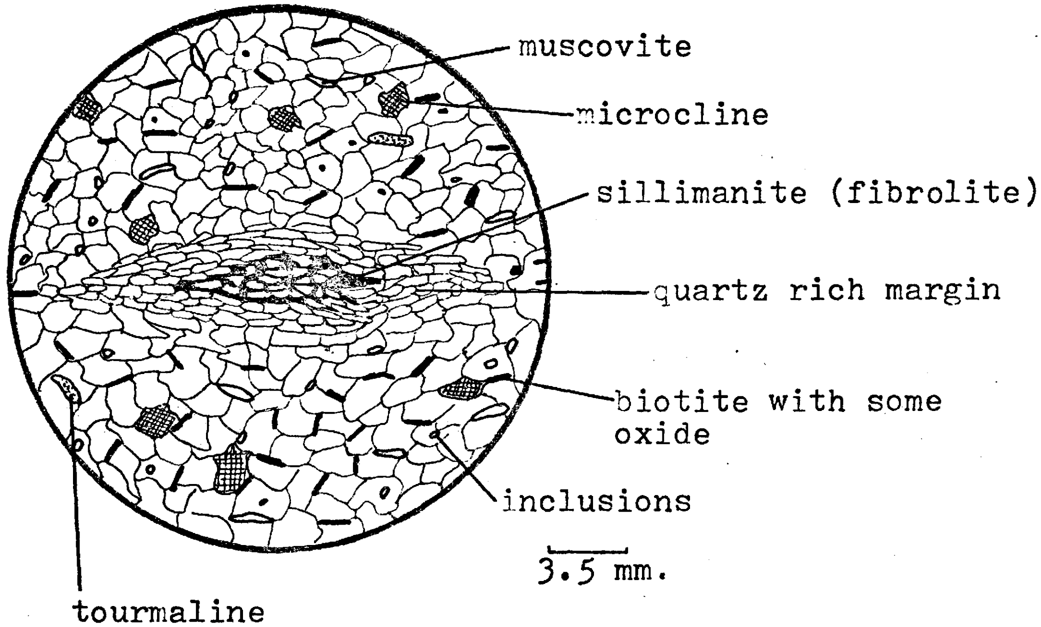

X-NICOLS

SAMPLE J73-061

Sample:	J73-006	UTM Coordinates:	379090	Easting
			7458120	Northing

Classification: Muscovite-Sillimanite Quartzite

Modal Abundances: Quartz -- 78%

Feldspar-K-spar -- 9% (Orthoclase)

-- 3% (Microcline)

Muscovite -- 5%

Sillimanite -- 5% (Fibrolite)

Textures:

The thin section is comprised of a quartz, K-spar and muscovite groundmass in which porphyroblasts of quartz, muscovite and sillimanite-fibrolite are found. The groundmass has four phases present, quartz, orthoclase, microcline and muscovite. The quartz grains are anhedral and show no preferred orientation but possess distinct grain boundaries. The grain boundaries are not smooth but very irregular and some grains show internal fracturing. Undulose extinction and inclusions of the other three phases are commonly observed. Grain sizes vary from 0.3 mm to 2.0 mm. The orthoclase grains are subhedral to anhedral but not as heavily fractured. Again, no preferred orientation is observed, but undulose extinction and anhedral inclusions of the three other phases occur. Grain sizes range from 0.2 mm to 1.8 mm. The microcline grains are subhedral to anhedral in form and show typical grid-iron twinning. These grains tend not to have any inclusions but possess fractures that are filled with anhedra of the other three phases present. The microcline grains are equidimensional and range in size from 0.1 mm to 0.5 mm. No alteration of the above three phases is observed.

The muscovite grains present in the groundmass material are subhedral to anhedral. The larger muscovite grains show embayments of both quartz and K-spar, however, no alteration products are observed. Grain boundaries are distinct and many of the smaller grains either occur as inclusions, or, in the case of the more blade-shaped grains, tend to cut grains of the other three phases. Grain sizes of the muscovite range from 0.1 mm to 0.9 mm.

The porphyroblasts are distinctive in that they are not only large (7.0 mm to 2.2 cm), but contain a nucleus rich in sillimanite-fibrolite and muscovite with a margin of quartz surrounding it. The quartz grains in the margin are anhedral and closely packed but show a preferred orientation parallel to the long axis of the porphyroblast. The muscovite present is subhedral to anhedral and shows embayments of quartz, some K-spar and alteration to sillimanite. The amount of K-spar in the porphyroblast is minimal as the stained slab sample indicates. Grain sizes in the porphyroblast tend to be larger than the groundmass varying from 0.4 mm to 2.0 mm.

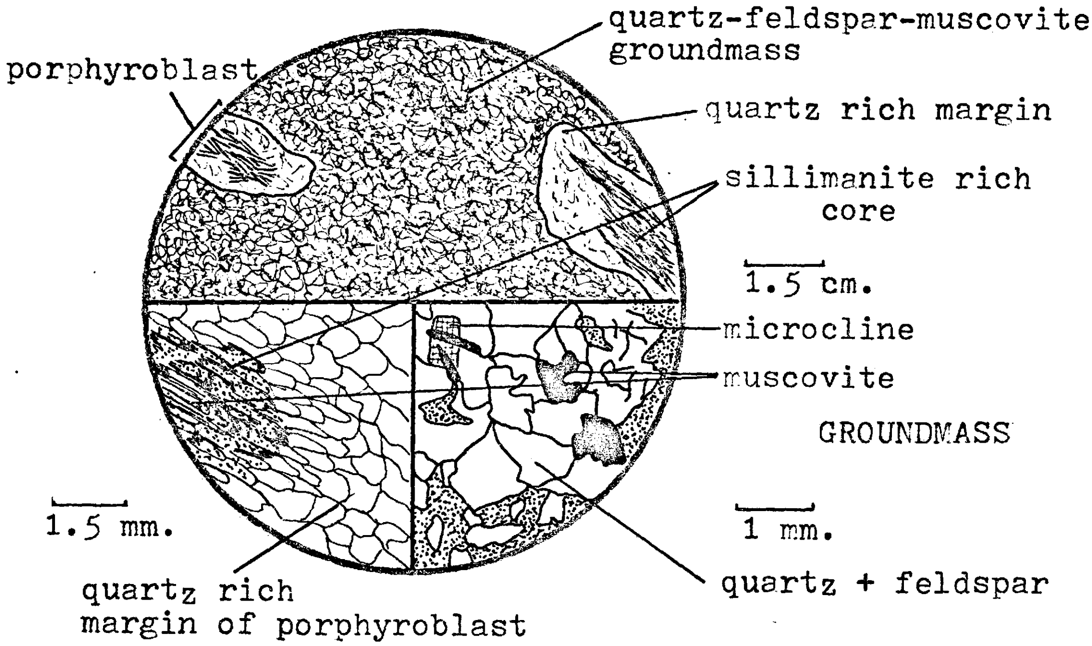

X-NICOLS

SAMPLE J73-006

Sample: J73-007 UTM Coordinates: 380000 Easting

7457300 Northing

Classification: Fuchsitic Quartzite

Modal Abundances: Quartz -- 93%

Muscovite -- 7% (Fuchsite)

Textures:

The thin section is comprised mostly of quartz and minor muscovite (fuchsite). The quartz grains are subhedral to anhedral and range in grain size from 0.1 mm to 3.0 mm, however, the majority of the quartz grains are greater than 0.5 mm. Most quartz grains show undulose extinction and no preferred orientation of the grains is observed. However, the grain boundaries of the quartz grains are sharp and occasionally meet at triple point junctions. Few such junctions show straight boundaries and most are undulating but not sutured.

The muscovite (fuchsite) grains are subhedral to anhedral and show no preferred orientation. Grain boundaries are distinct and no alteration occurs. These grains tend to lack inclusions although minor anhedra of quartz can be found in some grains. Grain sizes range from 0.4 mm to 1.8 mm.

Hence, the rock may be described as a fuchsitic quartzite displaying a granoblastic polygonal texture.

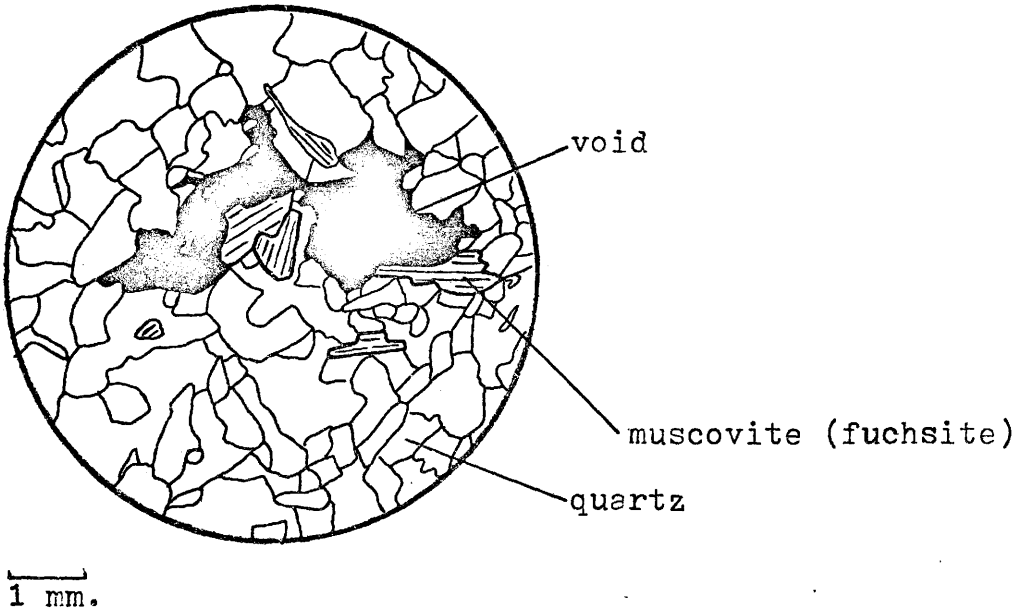

X-NICOLS

SAMPLE J73-007

Sample: J73-034 UTM Coordinates: 433560 Easting
7481480 Northing

Classification: Muscovite-Sillimanite Quartzite

Modal Abundances: Quartz -- 62%
Feldspar-K-spar -- 12% (Orthoclase)
Muscovite -- 12%
Sillimanite -- 14% (Fibrolite)

Textures:

The thin section is comprised of quartz and feldspar with microporphyroblasts of sillimanite-fibrolite and muscovite. The quartz and K-spar grains form the bulk of the slide. Both types of grains are anhedral and display sutured grain boundaries. Between some of the grains a fine grained mélange of anhedral quartz and orthoclase is found. Both of these features are probably a result of a slight post-crystalline deformation. No alteration of either phase is found and grain sizes range between 0.4 mm and 4.7 mm for the larger material, and 0.02 mm and 0.1 mm for the intergranular material. Quartz and K-spar grains also show undulose extinction.

The muscovite grains tend to be subhedral to anhedral and often show alteration to sillimanite-fibrolite. The sillimanite-fibrolite sometimes forms knots or porphyroblasts of radiating blocks of muscovite which have been altered to sillimanite-fibrolite wisps. The grain size of the porphyroblasts ranges from 0.3 mm to 3.4 mm.

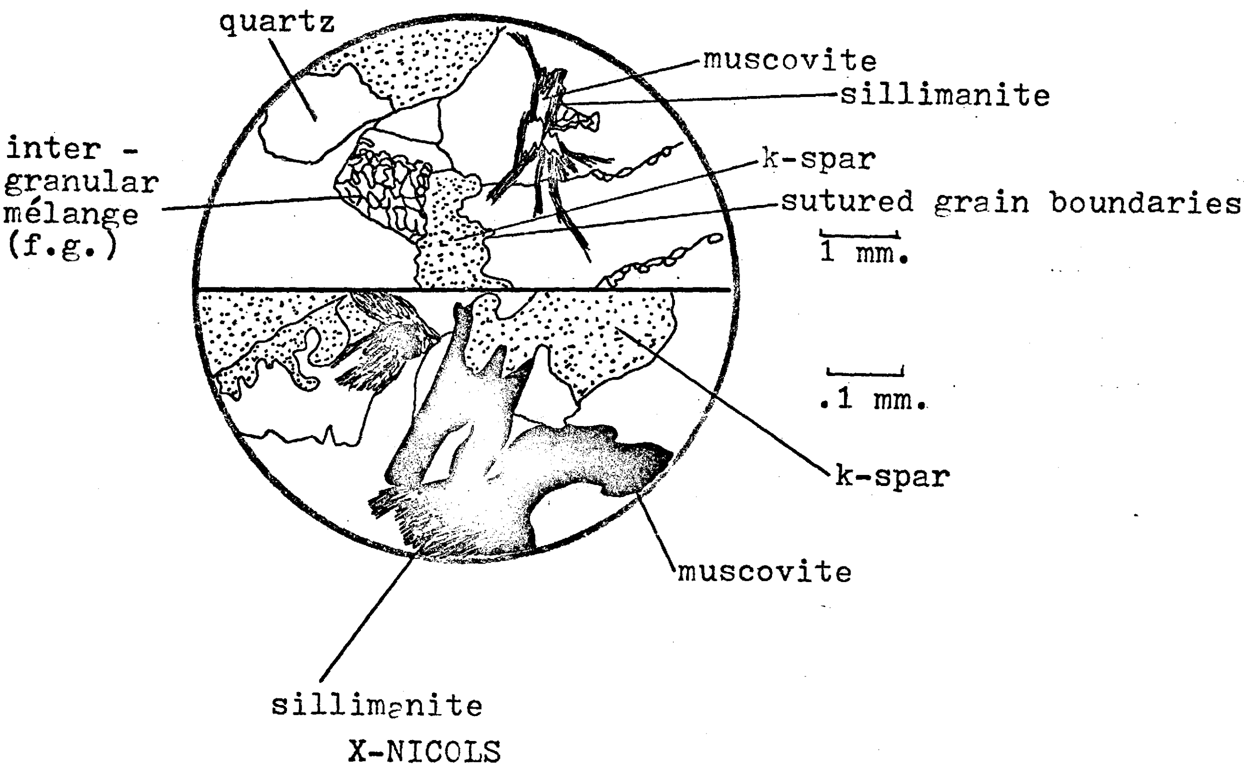

SAMPLE J73-034

Sample: J73-055 UTM Coordinates: 425480 Easting

7473250 Northing

Classification: Meta-Amphibolite

Modal Abundances: Feldspar-Plagioclase -- less than 1%

Biotite -- 10%

Hornblende -- 46%

Tremolite -- 16%

Diopside -- 5%

Calcite -- 15%

Siderite -- 1%

Sericite -- 3%

Tourmaline -- 2% (Schorlite)

Zircon -- less than 1%

Textures:

The thin section is composed of randomly oriented grains of amphibole, biotite and diopside, with a host of minor minerals including plagioclase, sericite, calcite, siderite, tourmaline and zircon. The amphibole grains include both tremolite and hornblende. These grains are subhedral to anhedral showing distinctive cleavage and straight grain boundaries. Some grains display a poikilitic texture with anhedral inclusions of very fine grained calcite present. Grain sizes of the amphiboles range from 0.4 mm to 3.4 mm for cross sections and 0.4 mm to 5.0 mm for longitudinal sections. No preferred orientation of these grains is observed.

The biotite grains occur as thin, randomly oriented, subhedral to anhedral, discontinuously layered blades. These blades sometimes cut amphibole grains and may be inclined to cleavage. Although no foliation is immediately obvious, a weak foliation is present in the hand specimen. Minor alteration to a dark brown-black mafic oxide is seen, but few zircons are present. Grain sizes of the biotite range from 1.5 mm to 2.1 mm.

Diopside occurs as subhedral to anhedral grains closely associated with amphibole but clearly distinct from it. The diopside grains show no alteration or inclusions and vary in grain size from 0.9 mm to 3.5 mm.

The siderite present occurs both as anhedra and as euhedral twinned rhombs. Some siderite grains show minor alteration to a brownish mafic oxide. Grain sizes range from 0.5 mm to 1.2 mm.

The calcite material is anhedral and extremely fine grained. It is associated with sericite and anhedral microlithic remnants of plagioclase, which are altered to such an extent that Michel-Levy tests are impossible. It is possible that the calcite and sericite are the alteration products of a relict calcic plagioclase. Some calcite also occurs as inclusions in poikilitic amphiboles as mentioned above.

Tourmaline (schorlite) occurs as subhedral to anhedral cross sections which have definite grain boundaries, but are highly fractured. These grains are approximately 1.0 mm in size.

Texturally, this rock may be described as a decussate amphibolite with subidioblastic hornblende, biotite and diopside grains.

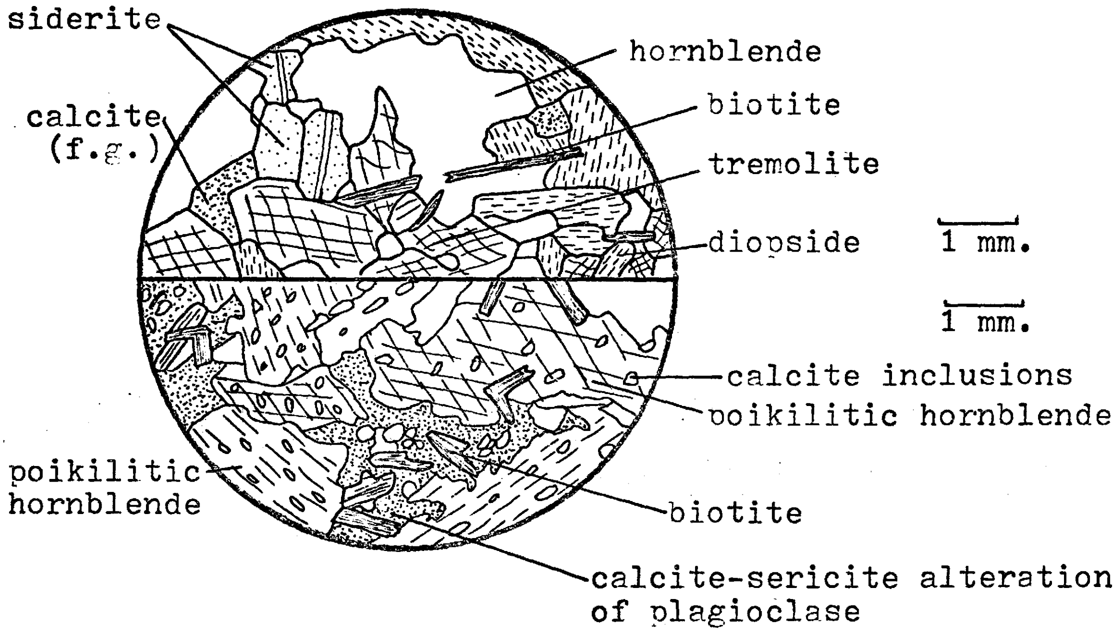

X-NICOLS

SAMPLE J73-055

Sample: J73-088 UTM Coordinates: 447950 Easting
7491370 Northing

Classification: Meta-Amphibolite

Modal Abundances: Quartz -- 5%

Feldspar -- 1%

Biotite -- 5%

Hornblende -- 10%

Tremolite -- 12%

Amphibolitic Groundmass -- 64%

Pyroxene -- 3%

Textures:

The thin section is comprised of hornblende and tremolite plus biotite in a groundmass of amphibolitic material with minor quartz and feldspar. The hornblende and tremolite grains are subhedral to euhedral and are the largest grains distinguishable in the groundmass. The tremolite occurs as long, continuous, but fractured blades, while the hornblende grains are more prismatic, but also fractured. Grain sizes range from less than 1.0 mm to approximately 22 mm for tremolite, while hornblende grains are seldom greater than 0.5 mm. Both of the above amphiboles are corroded by small anhedral quartz and feldspar grains, and are sometimes altered along cleavage planes and fractures to other amphiboles and biotite.

Biotite is minor in the thin section and cuts the amphiboles mentioned above. It is subhedral to anhedral and may include small anhedra of quartz. The biotite is often strained and varies in size from 0.05 mm to 2.0 mm. Since some of the biotite is formed by alteration of hornblende it is not surprising to find highly corroded inclusions of hornblende in the biotite.

The pyroxene present is subhedral and has indistinct grain boundaries, plus many fractures. Most important, it is highly altered to tremolite and corrosion by quartz is observed. Pyroxene grains range from 0.8 mm to 1.5 mm in size.

The quartz and feldspar grains are very minute anhedra (less than 0.1 mm), and often masked by minerals they corrode. The groundmass of amphibolitic material is fine grained (less than 0.1 mm), and anhedral. The groundmass displays a preferred orientation parallel to the larger tremolite blades, which define the foliation. The material in the groundmass is very difficult to analyse by optical methods.

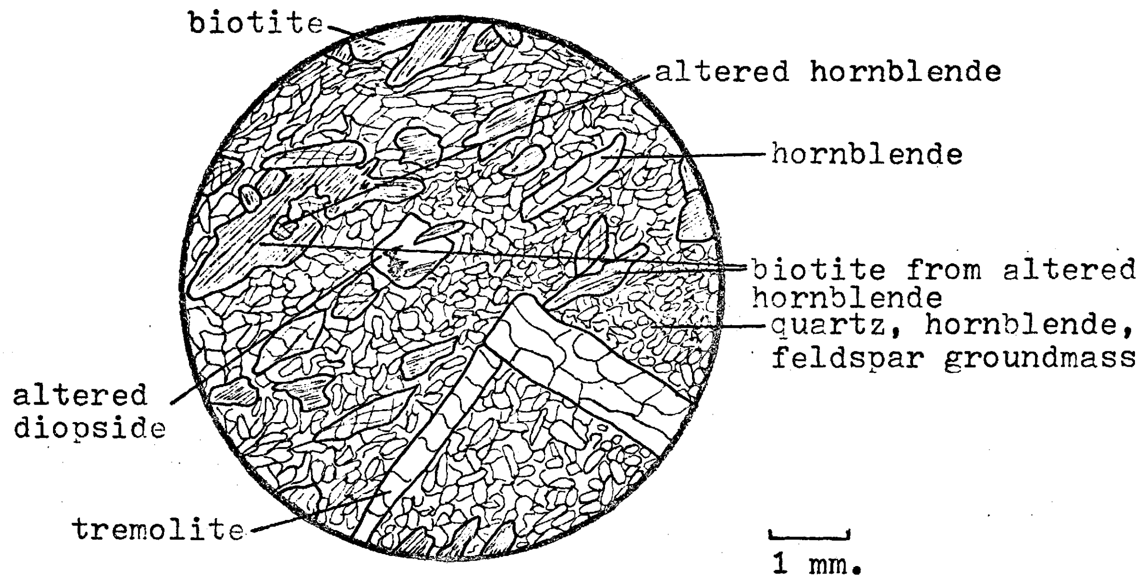

X-NICOLS

SAMPLES J73-088

Sample: J73-014 UTM Coordinates: 384500 Easting
7459030 Northing

Classification: Banded Quartz-Magnetite Iron Formation

Modal Abundances: Quartz -- 49%

Feldspar-K-spar -- 6%

Hornblende -- 12%

Pyroxene -- 8%

Mafic Oxide -- 25% (includes magnetite at least in part)

Textures:

The thin section is composed of layers of fine grained quartz (0.1 mm to 0.4 mm), fine grained hornblende and pyroxene (0.4 mm to 1.0 mm), separated by a layer of coarser grained quartz and K-spar (0.6 mm to 7.0 mm). The first two layers contain the highest concentration of fine grained mafic oxide. The fine grained quartz layer contains anhedral quartz with irregular but smooth grain boundaries and can be described as granoblastic. Minor anhedra of hornblende are dispersed in this layer also.

The hornblende-pyroxene layer contains anhedral large corroded grains of each mineral. Grain characteristics are heavily masked by black oxide material. However, interlayered with the hornblende-pyroxene-mafic oxide grains is fine grained quartz anhedra completely analogous to that mentioned above. Feather alteration of hornblende to red-brown oxide occurs along fractures.

The coarser grained quartz layer between the fine grained quartz and the hornblende layers contains anhedra of K-spar and quartz plus a few large anhedral grains of hornblende (0.2 mm to 1.8 mm), and a number of smaller dispersed grains of hornblende. The K-spar and quartz are anhedral and possess poorly sutured grain boundaries, suggesting post-crystalline deformation. Also, undulose extinction is common in this layer.

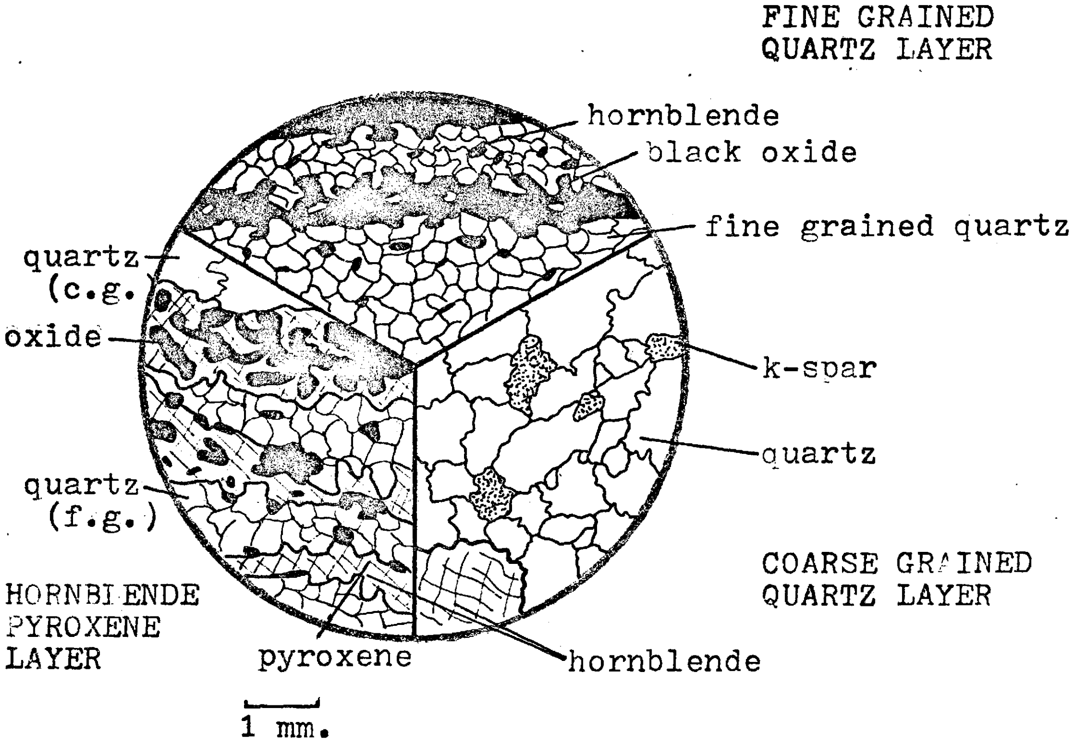

X-NICOLS

SAMPLE J73-014

APPENDIX B

RAW PETROCHEMICAL DATA

WHOLE ROCK ANALYSIS

IN

WEIGHT % OXIDES (UNNORMALIZED)

Samples	SiO_2	Al_2O_3	Fe (total)	MgO	CaO	NaO	K_2O	TiO_2	MnO	P_2O_5	Total
Greywacke-Paragneiss											
J73-032	77.32	12.21	4.21	1.70	1.47	0.35	2.26	0.36	0.05	0.09	100.01
-036	66.41	16.60	4.48	1.92	2.58	4.61	2.62	0.58	0.06	0.14	100.01
-040	85.50	7.95	1.92	0.62	2.51	0.35	0.91	0.15	0.02	0.04	99.98
-051	63.86	15.31	7.20	4.09	2.51	3.46	2.58	0.73	0.10	0.12	99.97
-050-2	62.66	15.13	9.30	3.69	1.91	3.48	2.98	0.68	0.20	0.04	100.06
-048	59.60	17.62	8.98	4.84	1.36	1.88	4.59	0.80	0.09	0.07	99.83
-004	53.55	8.97	15.35	10.71	6.60	0.33	3.30	0.82	0.22	0.24	100.09
-015	53.66	8.29	15.85	10.42	6.68	0.42	3.12	0.86	0.22	0.26	99.79

Continued.......

WHOLE ROCK ANALYSIS IN WEIGHT % OXIDES (UNNORMALIZED) -- Continued

Quartzite											
J73-006	90.90	5.92	0.28	0.05	0.04	0.22	2.56	0.06	0.01	0.02	100.05
-007	94.25	4.18	0.30	0.06	0.02	0.07	1.04	0.07	0.01	0.01	100.00
-034	90.52	9.05	0.24	0.03	0.02	0.02	0.07	0.03	0.01	0.01	100.00
Meta-Ultra-basic											
J73-055	49.61	10.62	14.25	12.41	10.47	0.44	1.43	0.47	0.24	0.08	100.01
-088	50.94	8.21	17.57	15.37	6.11	0.75	0.26	0.46	0.25	0.07	99.85

APPENDIX C

DATA REDUCTION PROGRAM

```
      PROGRAM TRIMOD (INPUT,OUTPUT,TAPE5=INPUT,TAPE6=OUTPUT)              WLF     1
C                                     BY                                 WLF     2
C                                  JM WOLFF                              WLF     3
C                                                                        WLF     4
C                                  MCMASTER UNIVERSITY                   WLF     5
C                                  APRIL 8, 1974                         WLF     6
C                                                                        WLF     7
C     THIS PROGRAM IS A MODIFICATION OF PROGRAM TRIANG WRITTEN BY        WLF     8
C     BERNARD M. GUNN,COPYRIGHT, FORTRAN COPY NUMBER 2.                  WLF     9
C                                                                        WLF    A9
C     THIS PROGRAM PLOTS  1). BINARY PLOTS,   ALKS/SIO2    ALKS/MGO      WLF    B9
C                                             ALKS/FEMG    NA2O/AL2O3    WLF    C9
C                                             K2O/AL2O3    MGO/AL2O3     WLF    D9
C                                             CAO/AL2O3    POT/SODA      WLF    E9
C                                             MGO/CAO      MGO/K2O       WLF    F9
C                         2). TERNARY PLOTS,  FER/NA,K/MGO               WLF    G9
C                                             CAO/NA2O/K2O               WLF    H9
C                                             NA,K/FE,MG/AL2O3           WLF    I9
C                                             AL2O3/K2O/NA2O             WLF    J9
C                                             A / F / M                  WLF    K9
C                                             A / C / F                  WLF    L9
C                                                                        WLF    M9
C                                                                        WLF    N9
      DIMENSION SI(200)                                                  PLT    10
      DIMENSION AL(200),FER(200),FE(200),CA(200),FM(200),ALK(200)        PLT    11
      DIMENSION ALK1(200),FM1(200),CA1(200),ALK2(200),WT(12),CON(12)     PLT    12
      REAL NI                                                            PLT    13
      REAL MN(200),MG(200),NA(200),K(200),MF(200),MG1,NA1(200),K1,MF1(20PLT    14
     20)                                                                 PLT    15
      DIMENSION NI(200), CR(200), CU(200),ZN(200), GA(200), RB(200),     PLT    16
     2 SR(200), BA(200), PB(200), TH(200), Y(200), CO(200)               PLT    17
      DIMENSION ALK3(200),K3(200),AW(200),FW(200),MW(200),AX(200),CX     WLF   A17
     2(200),FX(200),P(200),FQ(200),AQ(200),CN(200),AN(200)               WLF   B17
      REAL NA3,MG1,FN1                                                   WLF   C17
      INTEGER CAO,AL2O3,TITLE(8),PROJ(8)                                 PLT    18
      INTEGER ALKS, SIO2                                                 PLT    19
      INTEGER A,F,M,C                                                    WLF   A19
      TENTEN=10**10                                                      WLF   B19
      DATA(IALK=4HNA,K),(IFER=3HFER),(MGO=3HMGO),(CAO=3HCAO),(NA2O=4HNA2PLT    20
     2O),(K2O=3HK2O),(AL2O3=5HAL2O3),(IMF=5HFE,MG)                       PLT    21
      DATA(A=3H  A),(F=1HF),(M=1HM),(C=1HC)                              WLF   A21
      WRITE (6,900)
  900 FORMAT (1HS)
      WRITE(6,899)
  899 FORMAT(1HQ)
    1 FORMAT(7A10,A6,4I1)                                                PLT    22
    2 FORMAT(A5,2X,7A10,A2)                                              PLT    23
    3 FORMAT(A5,2X,12F6.3)                                               PLT    24
    4 FORMAT(A5,2X,12F6.1)                                               PLT    25
   11 FORMAT(1H1////10X,8A10//)                                          PLT    26
```

```
   12 FORMAT(/10X,A6,2X,8A10)                                          PLT   27
   13 FORMAT ( 10X,A6,2X,4F8.3,15X,3F8.3,15X,4F8.3 )                   PLT   28
   14 FORMAT(20X,3(F6.3,2X),23X,3(F6.3,2X),18X,3(F6.3,2X))             PLT   29
   15 FORMAT(//25X,7A10,A6)                                            PLT   30
   16 FORMAT(1X,*1RST LINE SAMPLE     FE2O3     FEO      MNO      MGO*,20X,*PLT   31
     2CAO      NA2O       K2O*,19X,*AL2O3  ALKALIS  FM+MN   FE+MG*)    PLT   32
   17 FORMAT(1X,*2ND LINE*,12X,*TRIANGLE ALK,FE+MN,MG*,28X,*TRIANGLE NA,PLT   33
     2CA,K*,20X,*TRIANGLE FE+MG,ALK,AL*)                               WLF   34
   18 FORMAT(/10X, *NO OF SAMPLES READ = *,I6//)                       PLT   35
  601 FORMAT(////1X,*1RST LINE SAMPLE      AL2O3    K2O     NA2O*,18X,*  WLF  A35
     2AL2O3      K2O      NA2O      CAO      FEO      MGO*)            WLF  B35
  602 FORMAT(1X,*2ND LINE*,12X,*TRIANGLE AL2O3,K2O,NA2O*,18X,*TRIANGLE  WLF  C35
     2AL2O3-NA2O-K2O-CAO,FEO,MGO*)                                     WLF  D35
  603 FORMAT(10X,A6,2X,3F8.3,19X,6F8.3)                                WLF  E35
  604 FORMAT(20X,3(F6.3,2X),19X,3(F6.3,2X))                            WLF  F35
  605 FORMAT(20X,3(F6.3,2X),19X,*A F M PLOT NOT COMPATIBLE WITH DATA GIVWLF  G35
     2EN*)                                                             WLF  H35
  607 FORMAT(////1X,*1RST LINE SAMPLE       AL2O3     FEO       K2O      NA2O WLF  I35
     2  CAO        P2O5     MGO       MNO*)                            WLF  J35
  608 FORMAT(1X,*2ND LINE*,12X,*TRIANGLE  AL2O3-NA2O-K2O,CAO-P2O5,FEO+MGWLF  K35
     2O+MNO*)                                                          WLF  L35
  609 FORMAT(10X,A6,2X,4F8.3,4F8.3)                                    WLF  M35
  610 FORMAT(20X,3(F6.3,2X),/1H1)                                      WLF  N35
  611 FORMAT(20X,*A C F PLOT NOT COMPATIBLE WITH DATA GIVEN*,/1H1)     WLF  O35
   20 NUM=J=0                                                          PLT   36
  100 READ 1, PROJ,NT,NM,NTR,NP                                        PLT   37
      PRINT 11, PROJ                                                   PLT   38
C     PRINT 16, PRINT 17                                               PLT   39
  110 CONTINUE                                                         PLT   40
      IF(NT.EQ.0) GO TO 120                                            PLT   41
      READ 2,N1, TITLE                                                 PLT   42
      IF(N1.EQ.6HCHANGE) GO TO 1000                                    PLT   43
      IF(N1.EQ.6HFINISH) GO TO 1000                                    PLT   44
C     PRINT 12, N1, TITLE                                              PLT   45
  120 READ 3, N2, (WT(I), I=1,12)                                      PLT   46
      IF(N2.EQ.6HCHANGE) GO TO 1000                                    PLT   47
      IF(N2.EQ.6HFINISH) GO TO 1000                                    PLT   48
      J=J+1                                                            PLT   49
      AL(J)=WT(2)$FER(J)=WT(4)$FE(J)=WT(5)                             PLT   50
      SI(J)=WT(1)                                                      PLT   51
      MN(J)=WT(6)$ MG(J)=WT(7)$ CA(J)=WT(8)$ NA(J)=WT(9)$ K(J)=WT(10)  PLT   52
      FM(J)=FER(J)+FE(J)+MN(J)                                         PLT   53
      P(J)=WT(11)                                                      WLF  A53
      ALK(J)=K(J)+NA(J)                                                PLT   54
      MF(J)=FER(J)+ FE(J)+MG(J)                                        PLT   55
      IF(NTR.EQ.0.)GOTO 105                                            PLT   56
      READ 4, N3, CR(J),NI(J),CU(J),ZN(J),GA(J),RB(J),SR(J),BA(J),PB(J),PLT   57
     2TH(J), Y(J), CO(J)                                               PLT   58
  105 CALL TPC(FM(J),ALK(J),MG(J),FM1(J),ALK1(J),MG1)                  PLT   59
      CALL TPC(CA(J),NA(J),K(J),CA1(J),NA1(J),K1)                      PLT   60
      CALL TPC(ALK(J),MF(J),AL(J),ALK2(J),MF1(J),AL1)                  PLT   61
      CALL TPC(AL(J),K(J),NA(J),ALK3(J),K3(J),NA3)                     WLF  A61
      CALL AFM(AL(J),FER(J),K(J),MG(J),NA(J),CA(J),AW(J),FW(J),MW(J))  WLF  B61
      IF(AW(J).EQ.TENTEN)GOTO204                                       WLF  C61
```

```
      CALL TPC(AW(J),FW(J),MW(J),AQ(J),FQ(J),MQ1)                       WLF  D61
  204 CALL ACF(AL(J),FER(J),K(J),NA(J),CA(J),P(J),MG(J),MN(J),AX(J),    WLF  E61
     2CX(J),FX(J))                                                      WLF  F61
      IF(AX(J).EQ.TENTEN)GOTO111                                        WLF  G61
      CALL TPC(AX(J),CX(J),FX(J),AN(J),CN(J),FN1)                       WLF  H61
  111 NUM=NUM+1                                                         PLT   62
      PRINT 16 $ PRINT 17                                               WLF  A62
      PRINT 12, N1, TITLE                                               WLF  B62
      PRINT 13,N2,FER(J),FE(J),MN(J),MG(J),CA(J),NA(J),K(J),AL(J),ALK(J)PLT   63
     2,FM(J),MF(J)                                                      PLT   64
      PRINT 14,ALK1(J),FM1(J),MG1,NA1(J),CA1(J),K1,MF1(J),ALK2(J),AL1   PLT   65
      PRINT 601                                                         WLF  A65
      PRINT 602                                                         WLF  B65
      PRINT 12,N1,TITLE                                                 WLF  C65
      PRINT 603,N2,AL(J),K(J),NA(J),AL(J),K(J),NA(J),CA(J),FER(J),MG    WLF  D65
     2(J)                                                               WLF  E65
      IF(AW(J).EQ.TENTEN)GOTO270                                        WLF  F65
      PRINT 604,ALK3(J),K3(J),NA3,AQ(J),FQ(J),MQ1                       WLF  G65
      GOTO271                                                           WLF  H65
  270 PRINT 605,ALK3(J),K3(J),NA3                                       WLF  I65
  271 PRINT 607                                                         WLF  J65
      PRINT 608                                                         WLF  K65
      PRINT 12,N1,TITLE                                                 WLF  L65
      PRINT 609,N2,AL(J),FER(J),K(J),NA(J),CA(J),P(J),MG(J),MN(J)       WLF  M65
      IF(AX(J).EQ.TENTEN)GOTO275                                        WLF  N65
      PRINT 610,AN(J),CN(J),FN1                                         WLF  O65
      GOTO130                                                           WLF  P65
  275 PRINT 611                                                         WLF  Q65
  130 GO TO 110                                                         PLT   66
 1000 CONTINUE                                                          PLT   67
      N=NUM                                                             PLT   68
      PRINT 18, N                                                       PLT   69
      CALL XYPLT(SI,ALK,4HSIO2,4HALKS,NUM)                              PLT   70
      PRINT 15, PROJ                                                    PLT   71
      CALL XYPLT(MG,ALK,3HMGO,4HALKS,NUM)                               PLT   72
      CALL XYPLT(MF,ALK,4HFEMG,4HALKS,NUM)                              PLT   73
      CALL XYPLT(AL,NA,5HAL2O3,4HNA2O,NUM)                              PLT   74
      PRINT 15, PROJ                                                    PLT   75
      CALL XYPLT(AL,K,5HAL2O3,3HK2O,NUM)                                PLT   76
      CALL XYPLT(AL,MG,5HAL2O3,3HMGO,NUM)                               PLT   77
      CALL XYPLT(AL,CA,5HAL2O3,3HCAO,NUM)                               PLT   78
      CALL XYPLT(NA,K,4HSODA,3HPOT,NUM)                                 PLT   79
      PRINT 15,PROJ                                                     PLT   80
      CALL XYPLT(CA,MG,3HCAO,3HMGO,NUM)                                 PLT   81
      CALL XYPLT(K,MG,3HK2O,3HMGO,NUM)                                  PLT   82
      PRINT 15, PROJ                                                    PLT   83
      IF (NTR.EQ.J) GO TO 777                                           PLT   84
      CALL XYPLT(K,RB,3HK2O,2HRB,NUM)                                   PLT   85
      PRINT 15, PROJ                                                    PLT   86
      CALL XYPLT(K,BA,3HK2O,2HBA,NUM)                                   PLT   87
      PRINT 15, PROJ                                                    PLT   88
      CALL XYPLT (NA,SR,4HNA2O,2HSR,NUM)                                PLT   89
      PRINT 15, PROJ                                                    PLT   90
```

```
  777 CALL TERNRY(ALK1,FM1,IALK,IFER,MGO,NUM,MG)                          PLT   91
      PRINT 15,PROJ                                                        PLT   92
      CALL TERNRY(NA1,CA1,NA2O,CAO,K2O,NUM,K)                              PLT   93
      PRINT 15,PROJ                                                        PLT   94
      CALL TERNRY(MF1,ALK2,IMF,IALK,AL2O3,NUM,AL)                          PLT   95
      PRINT 15,PROJ                                                        PLT   96
      CALL TERNRY(K3,ALK3,K2O,AL2O3,NA2O,NUM,NA)                           WLF  A96
      PRINT 15,PROJ                                                        WLF  B96
      CALL TERNRY (FQ,AQ,F,A,M,NUM,MQ1)                                    WLF  C96
      PRINT 15,PROJ                                                        WLF  D96
      CALL TERNRY(CN,AN,C,A,F,NUM,FN1)                                     WLF  E96
      PRINT 15,PROJ                                                        WLF  F96
      IF(N1.EQ.6HCHANGE) GO TO 20                                          PLT   97
      IF(N2.EQ.6HCHANGE) GO TO 20                                          PLT   98
 2000 STOP                                                                 PLT  101
      END                                                                  PLT  102

SUBROUTINE TPC        73/73   OPT=0   TRACE            FTN 4.0+P355     04/08/74  15.38.2

      SUBROUTINE TPC (A,B,C,A1,B1,C1)                                      PLT  103
C     COMPUTATION OF RELATIVE PERCENTAGES IN A TRIPOLAR PROJECTION.        PLT  104
      TOTAL=A+B+C                                                          PLT  105
      IF(TOTAL.EQ.0.) GO TO 1                                              PLT  106
      A1=A*100./TOTAL                                                      PLT  107
      B1=B*100./TOTAL                                                      PLT  108
      C1=100.-A1-B1                                                        PLT  109
      GO TO 2                                                              PLT  110
    1 A1=B1=C1=0.                                                          PLT  111
    2 RETURN                                                               PLT  112
      END                                                                  PLT  113

SUBROUTINE TERNRY     73/73   OPT=0   TRACE            FTN 4.0+P355     04/08/74  15.38.2

      SUBROUTINE TERNRY (A,B,ANAME,BNAME,CNAME,N,C)                        PLT  114
C                                                                          PLT  115
C        WRITTEN BY GEOCHEMISTRY SECTION OF CANADIAN GEOLOGICAL SURVEY.    PLT  116
C                                                                          PLT  117
      DIMENSION A(N),B(N),AREA(51,101),HOL(38),C(N)                        PLT  118
      INTEGER ANAME, BNAME, CNAME                                          PLT  119
      INTEGER AREA,HOL                                                     PLT  120
      DATA  HOL/1H*,1H2,1H3,1H4,1H5,1H6,1H7,1H8,1H9,1HA,1HB,1HC,1HD,1HE,PLT  121
     1          1HF,1HG,1HH,1HI,1HJ,1HK,1HL,1HM,1HN,1HO,1HP,1HQ,1HR,1HS,PLT  122
     2          1HT,1HU,1HV,1HW,1HX,1HY,1HZ,1H$,1H ,1H+/                  PLT  123
C                                                                          PLT  124
C     PROGRAM TO PLOT TERNARY DIAGRAMS                                     PLT  125
      DO 1 I=1,51                                                          PLT  126
      DO 1 J=1,101                                                         PLT  127
    1 AREA(I,J)=0                                                          PLT  128
C                                                                          PLT  129
      DO 2 K=1,N                                                           PLT  130
      IF(A(K).GT.0.) GO TO 10                                              PLT  131
      IF(B(K).GT.0.) GO TO 10                                              PLT  132
      IF(C(K).EQ.0.) GO TO 2                                               PLT  133
      AREA(51,101)=AREA(51,101)+1                                          PLT  134
```

```
      GO TO 2
   10 ACOMP=100.0-A(K)
      ACOMP2=ACOMP/2.0
      Z=(B(K)-ACOMP2)/1.73205
      X=SQRT(ACOMP*ACOMP-ACOMP2*ACOMP2)-Z
      YC=100.-B(K)
      I=(YC+1.)/2.+1.
      J= X*0.8562+ 1.0
      AREA(I,J)=AREA(I,J)+1
    2 CONTINUE
C
      DO 4 I=1,51
      DO 4 J=1,101
      IF(AREA(I,J).GT.0)GO TO 3
      AREA(I,J)=HOL(37)
      GO TO 4
    3 K=AREA(I,J)
      IF(K.GE.36)K=36
      AREA(I,J)=HOL(K)
    4 CONTINUE
C
      J1=51
      DO 5 I=1,50,5
      J2=102-J1
      IF(AREA(I,J1).EQ.HOL(37))AREA(I,J1)=HOL(38)
      IF(AREA(I,J2).EQ.HOL(37))AREA(I,J2)=HOL(38)
    5 J1=J1-5
      DO 6 J=1,101,10
      IF(AREA(51,J).EQ.HOL(37))AREA(51,J)=HOL(38)
    6 CONTINUE
C
      WRITE (6,101) BNAME
      DO 7 I=1,50
    7 WRITE (6,102) (AREA(I,J),J=1,101)
      WRITE (6,103) ANAME,(AREA(51,J),J=1,101),CNAME
      RETURN
C
  101 FORMAT (1H1,54X,A5)
  102 FORMAT (1H ,6X,101A1)
  103 FORMAT (1H ,1X,A5,101A1,A5)
C
      END
```

SUBROUTINE XYPLT   73/73   OPT=0   TRACE   FTN 4.0+P355   04/08/74 15.38.30

```
      SUBROUTINE XYPLT(X1,Y1,XNAM,YNAM,NN)
C     PLOTS TWO VARIABLES ON LINE PRINTER, CALLS POLYNOM TO CALC R ETC.
      DIMENSION X(300), Y(300), PAGE(53,103), SIG(38)
      DIMENSION X1(NN), Y1(NN)
      INTEGER XNAM,YNAM,PAGE,SIG
      DATA SIG/1H*,1H2,1H3,1H4,1H5,1H6,1H7,1H8,1H9,1HA,1HB,1HC,1HD,1HE,
     21HF,1HG,1HH,1HI,1HJ,1HK,1HL,1HM,1HN,1HO,1HP,1HQ,1HR,1HS,1HT,1HU,1H
     2V,1HW,1HX,1HY,1HZ,1H-,1H ,1H+/
C
```

```
C     FILTER ZERO VALUES.                                               PLT  186
C                                                                       PLT  187
      J=1                                                               PLT  188
      DO 120 I=1,NN                                                     PLT  189
      IF(X1(I).LE.0.0) GO TO 120                                        PLT  190
      IF(Y1(I).LE.0.0) GO TO 120                                        PLT  191
      X(J)=X1(I)                                                        PLT  192
      Y(J)=Y1(I)                                                        PLT  193
      J=J+1                                                             PLT  194
  120 CONTINUE                                                          PLT  195
      N=J-1                                                             PLT  196
      CALL MAX(X,Y,XMIN,XMAX,YMIN,YMAX,N)                               PLT  197
      XN=XMIN                                                           PLT  198
      YN=YMIN                                                           PLT  199
      XMIN=YMIN=0.0                                                     PLT  200
      DO 100 I=1,53                                                     PLT  201
      DO 100 J=1,103                                                    PLT  202
  100 PAGE(I,J)=0                                                       PLT  203
      CALL POLYNOM(X,Y,N,R,SEE,RC,AA0,AA1,AA2)                          PLT  204
      DO 104 K=1,N                                                      PLT  205
      IF(X(K).EQ.0.0.OR.Y(K).EQ.0.0) GO TO 104                          PLT  206
      X(K)=X(K)-XMIN                                                    PLT  207
      Y(K)=Y(K)-YMIN                                                    PLT  208
      XSCALE=100.0/(XMAX-XMIN)                                          PLT  209
      YSCALE=50.0/(YMAX-YMIN)                                           PLT  210
      I=52.0-Y(K)*YSCALE+0.5                                            PLT  211
      J=X(K)*XSCALE+0.5                                                 PLT  212
      IF(I.LT.1) I=1                                                    PLT  213
      J=J+2                                                             PLT  214
      IF(J.LT.3) J=3                                                    PLT  215
      PAGE(I,J)=PAGE(I,J)+1                                             PLT  216
      IF(PAGE(I,J).GT.36) PAGE(I,J)=36                                  PLT  217
  104 CONTINUE                                                          PLT  218
    5 FORMAT(/20X,2I10)                                                 PLT  219
      DO 105 I=3,51                                                     PLT  220
      DO 105 J=3,101                                                    PLT  221
      K=PAGE(I,J)                                                       PLT  222
      PAGE(I,J)=SIG(K)                                                  PLT  223
  105 IF(PAGE(I,J).EQ.0) PAGE(I,J)=1H                                   PLT  224
      DO 101 I=1,53                                                     PLT  229
      PAGE(I,103)=1H+                                                   PLT  230
  101 PAGE(I,1)=1H+                                                     PLT  231
      DO 102 J=2,102                                                    PLT  232
      PAGE(1,J)=1H+                                                     PLT  233
  102 PAGE(53,J)=1H+                                                    PLT  234
      DO 106 I=2,52,10                                                  PLT  235
      PAGE(I,2)=1H-                                                     PLT  236
      PAGE(I,102)=1H-                                                   PLT  237
  106 CONTINUE                                                          PLT  238
      DO 107 J=2,102,10                                                 PLT  239
      PAGE(52,J)=1H+                                                    PLT  240
      PAGE(2,J)=1H+                                                     PLT  241
  107 CONTINUE                                                          PLT  242
```

```
      WRITE(6,5)YNAM,YMAX
      DO 108 I=1,53
      WRITE(6,2) (PAGE(I,J), J=1,103)
  108 CONTINUE
      XMED=XMAX/2.0
      WRITE(6,3) YMIN,XMIN,XMED,XMAX,XNAM
      PRINT 9, R, SEE
      PRINT 10, RC
    2 FORMAT(20X,103A1)
    3 FORMAT (13X,F4.1,2X,F4.1,44X,F5.1,46X,F5.1,/69X,A5)
    6 FORMAT(1H1, 5X,A5,2X,F5.1,8H PERCENT)
    9 FORMAT(/33X,*LINEAR CORRELATION COEFFICIENT R= *,F6.2,5X,*STANDARD
     2 ERROR OF ESTIMATE= *,F6.2)
   10 FORMAT(33X,*CURVILINEAR CORRELATION COEFFICIENT =*F6.4)
      RETURN
      END
```

SUBROUTINE MAX 73/73 OPT=0 TRACE FTN 4.0+P355 04/08/74 15.38.33.

```
      SUBROUTINE MAX(X,Y,XMIN,XMAX,YMIN,YMAX,N)
      DIMENSION X(N), Y(N)
      XMIN=YMIN=100.0
      XMAX=YMAX=0.0
      DO 100 I=1,N
      IF(X(I).LT.XMIN) XMIN=X(I)
      IF(X(I).GT.XMAX) XMAX=X(I)
      IF(Y(I).GT.YMAX) YMAX=Y(I)
      IF(Y(I).LT.YMIN) YMIN=Y(I)
  100 CONTINUE
      IF(XMAX.GT.100.0) GO TO 150
      IF(XMAX.LT.5.0)  XMAX=5.0
      IF  (XMAX.LT.10.0.AND.XMAX.GT.5.0) XMAX=10.0
      IF(XMAX.LT.25.0.AND.XMAX.GT.10.0)  XMAX=25.0
      IF(XMAX.LT.50.0.AND.XMAX.GT.25.0)  XMAX=50.0
      IF(XMAX.LT.80.0.AND.XMAX.GT.50.0)  XMAX=80.0
      IF(XMAX.LT.100..AND.XMAX.GT.80.0)  XMAX=100.0
      IF(YMAX.GT.100.0) GO TO 333
      IF(YMAX.LT.5.0) YMAX=5.0
      IF(YMAX.LT.10.0.AND.YMAX.GT.5.0)   YMAX=10.0
      IF(YMAX.LT.25.0.AND.YMAX.GT.10.0)  YMAX=25.0
      IF(YMAX.LT.50.0.AND.YMAX.GT.25.0)  YMAX=50.0
      IF(YMAX.LT.100..AND.YMAX.GT.50.0)  YMAX=100.0
      GO TO 600
  150 CONTINUE
      DO 200 K=1,1000
      IF((K*100).GT.XMAX) GO TO 300
  200 CONTINUE
  300 XMAX=K*100
  333 CONTINUE
      DO 400 K=1,1000
      IF((K*100).GT.YMAX) GO TO 500
  400 CONTINUE
  500 YMAX=K*100
```

```
  600 CONTINUE
    4 FORMAT(/20X,4HXMIN,5X,4HXMAX,5X,4HYMIN,5X,4HYMAX )
    5 FORMAT(/20X,4F10.2/)
      RETURN
      END
```

SUBROUTINE POLYNOM 73/73 OPT=0 TRACE FTN 4.0+P355 04/08/74 15.38.35

```
      SUBROUTINE POLYNOM(X,Y,N,R,SEE,RC,AA0,AA1,AA2)
      DIMENSION A(3), B(3), C(3), D(3)
      DIMENSION YEST(200)
      DIMENSION XY(200), XX(200), YY(200),X2(200), Y2(200)
      DIMENSION X(200), Y(200)
    7 FORMAT(//20X,*LINEAR CORRELATION COEFFICIENT = * F10.2)
      SX=0.0
      SY=0.0
      DO 150 I=1,N
      SX=SX+X(I)
      SY=SY+Y(I)
  150 CONTINUE
      XBAR=SX/N
      YBAR=SY/N
      SYY2=0.0
      DO 110 I=1,N
      YY(I)=Y(I)-YBAR
      SYY2=SYY2+YY(I)*YY(I)
  110 CONTINUE
      SX2Y=0.0
      SX2=0.0
      SX3=0.0
      SX4=0.0
      SY2=0.0
      SXY=0.0
      DO 120 I=1,N
      SXY=SXY+X(I)*Y(I)
      SX2=SX2+X(I)**2
      SY2=SY2+Y(I)**2
      SX2Y=SX2Y+X(I)**2*Y(I)
      SX3=SX3+X(I)**3
      SX4=SX4+X(I)**4
  120 CONTINUE
C      CALC OF R LINEAR CORRELATION COEFFICIENT.
      Z=N*SX2-SX**2
      A0=(SY*SX2-SX*SXY)/Z
      A1=(N*SXY-SX*SY)/Z
   10 FORMAT(/20X,*COEFFICIENTS A0 AND A1 = *, 2F10.4/)
C     SEE = STANDARD ERROR OF ESTIMATE.
      SEE=SQRT((SY2-A0*SY-A1*SXY)/(N-2))
    8 FORMAT(/20X, *LONG VERSION OF R (LINEAR) =*, F10.4,//)
       R=(N*SXY-SX*SY)/SQRT((N*SX2-SX*SX)*(N*SY2-SY*SY))
C
C     CALCULATION OF A CURVILINEAR FIT.
C
```

```
      A(1)=SY                                                           PLT  343
      A(2)=SXY                                                          PLT  344
      A(3)=SX2Y                                                         PLT  345
      B(1)=N                                                            PLT  346
      B(2)=SX                                                           PLT  347
      B(3)=SX2                                                          PLT  348
      C(1)=SX                                                           PLT  349
      C(2)=SX2                                                          PLT  350
      C(3)=SX3                                                          PLT  351
      D(1)=SX2                                                          PLT  352
      D(2)=SX3                                                          PLT  353
      D(3)=SX4                                                          PLT  354
      CALL COEF(A,B,C,D,NS,AA0,AA1,AA2)                                 PLT  355
   99 FORMAT(/20X,*COEFFICIENTS OF CURVE ARE *, 3F10.4)                 PLT  356
C     CALCULATION OF CURVILINEAR CORRELATION COEFFICIENT.               PLT  357
      SYED=0.0                                                          PLT  358
      DO 175 I=1,N                                                      PLT  359
      YEST(I)=AA0+AA1* X(I)+AA2*X(I)**2                                 PLT  360
      SYED=SYED  +(YEST(I)-YBAR)**2                                     PLT  361
  175 CONTINUE                                                          PLT  362
      RC=SQRT(SYED/SYY2)                                                PLT  363
      RETURN                                                            PLT  364
      END                                                               PLT  365
SUBROUTINE COEF        73/73    OPT=0    TRACE          FTN 4.0+P355      04/08/74  15.38.37

      SUBROUTINE COEF(A,B,C,D,NS,A0,A1,A2)                              PLT  366
      DIMENSION A(3), B(3), C(3), D(3)                                  PLT  367
      CALL D3(DT,B,C,D)                                                 PLT  368
      IF(ABS(DT).GT.0.0001) GO TO 1                                     PLT  369
      NS=1                                                              PLT  370
    2 FORMAT(/10X,*DETERMINATIVE FUNCTION INFINITELY SMALL*,//)         PLT  371
      PRINT 2                                                           PLT  372
      RETURN                                                            PLT  373
    1 NS=0                                                              PLT  374
      CALL D3(AA,A,C,D)                                                 PLT  375
      A0=AA/DT                                                          PLT  376
      CALL D3(AA,B,A,D)                                                 PLT  377
      A1=AA/DT                                                          PLT  378
      CALL D3(AA,B,C,A)                                                 PLT  379
      A2=AA/DT                                                          PLT  380
      RETURN                                                            PLT  381
      END                                                               PLT  382
SUBROUTINE D3          73/73    OPT=0    TRACE          FTN 4.0+P355      04/08/74  15.38.3

      SUBROUTINE D3(R,A,B,C)                                            PLT  383
      DIMENSION A(3), B(3), C(3)                                        PLT  384
      R=A(1)*(B(2)*C(3)-B(3)*C(2)) -B(1)*(A(2)*C(3)-C(2)*A(3)) + C(1)*(APLT  385
     2(2)*B(3)-B(2)*A(3))                                               PLT  386
      RETURN                                                            PLT  387
      END                                                               PLT  388
```

```
SUBROUTINE ACF          73/73    OPT=0    TRACE                    FTN 4.0+P355        04/08/74  15.38.40.

              SUBROUTINE ACF(A9,B9,C9,D9,E9,F9,G9,H9,AP,FP,CP)
C             CALCULATION ASSUMES FEO IS TOTAL IRON PRESENT
              A9P=A9/101.94
              B9P=B9/71.85
              C9P=C9/94.20
              D9P=D9/61.98
              E9P=E9/56.08
              F9P=F9/141.95
              G9P=G9/40.32
              H9P=H9/70.94
              AP=A9P-(D9P+C9P)
              CP=E9P-3.3*(F9P)
              FP=B9P+G9P+H9P
              IF(AP.LT.0.0.OR.FP.LT.0.0.OR.CP.LT.0.0)GOTO727
              RETURN
          727 AP=10**10
              RETURN
              END
SUBROUTINE AFM          73/73    OPT=0    TRACE                    FTN 4.0+P355        04/08/74  15.38.41.

              SUBROUTINE AFM(A8,B8,C8,D8,E8,F8,AY,BY,CY)
C             CALCULATION ASSUMES FEO TOTAL IRON-MAGNETITE-ILMENITE IGNORED
              A8P=A8/101.94
              B8P=B8/71.85
              C8P=C8/94.20
              D8P=D8/70.94
              E8P=E8/61.98
              F8P=F8/56.08
              AY=A8P-C8P-E8P-F8P
              BY=B8P
              CY=D8P
              IF(AY.LT.0.0.OR.BY.LT.0.0.OR.CY.LT.0.0)GOTO727
              RETURN
          727 AY=10**10
              RETURN
              END
```